Center for Flow Physics and Control

in the

Hessert Laboratory for Aerospace Research

University of Notre Dame
Notre Dame, IN 46556

Department of Aerospace and Mechanical Engineering

DISTRIBUTION STATEMENT A
Approved for Public Release
Distribution Unlimited

20070426200

Best Available Copy

REPORT DOCUMENTATION PAGE

Form Approved
OMB No. 0704-0188

The public reporting burden for this collection of information is estimated to average 1 hour per response, including the time for reviewing instructions, searching existing data sources, gathering and maintaining the data needed, and completing and reviewing the collection of information. Send comments regarding this burden estimate or any other aspect of this collection of information, including suggestions for reducing the burden, to Department of Defense, Washington Headquarters Services, Directorate for Information Operations and Reports (0704-0188), 1215 Jefferson Davis Highway, Suite 1204, Arlington, VA 22202-4302. Respondents should be aware that notwithstanding any other provision of law, no person shall be subject to any penalty for failing to comply with a collection of information if it does not display a currently valid OMB control number.
PLEASE DO NOT RETURN YOUR FORM TO THE ABOVE ADDRESS.

1. REPORT DATE *(DD-MM-YYYY)*	2. REPORT TYPE	3. DATES COVERED *(From - To)*
28-03-2007	Final Technical Report	01-01-2004 to 31-12-2006

4. TITLE AND SUBTITLE
Tip-Clearance Control Using Blade Mounted Plasma Actuators

5a. CONTRACT NUMBER
FA9550-04-1-0198

5b. GRANT NUMBER

5c. PROGRAM ELEMENT NUMBER

6. AUTHOR(S)
Scott C. Morris and Thomas C. Corke

5d. PROJECT NUMBER

5e. TASK NUMBER

5f. WORK UNIT NUMBER

7. PERFORMING ORGANIZATION NAME(S) AND ADDRESS(ES)
Department of Aerospace and Mechanical Engineering
University of Notre Dame

8. PERFORMING ORGANIZATION REPORT NUMBER
UND-SM07-0328

9. SPONSORING/MONITORING AGENCY NAME(S) AND ADDRESS(ES)
Air Force Office of Scientific Research
875 N. Randolf Street
Suite 324, Room 3112
Arlington, VA 22203-1768
Dr Rhett Jeffries/NA

10. SPONSOR/MONITOR'S ACRONYM(S)
AFRL-SR-AR-TR-07-0136

12. DISTRIBUTION/AVAILABILITY STATEMENT
Distribution Statement A: Public release; distribution Unlimited

13. SUPPLEMENTARY NOTES

14. ABSTRACT

This report documents experimental results from a series of experiments using active flow control to improve the performance and efficiency of turbine tip clearance flows. The flow control was based on plasma actuators. Two experimental facilities were used as part of this research project. The first was a low-speed, large-scale turbine cascade using Pak-B turbine blades. The second was a smaller scale, high-speed cascade with low aspect ratio. The active flow control was design to act as a "plasma squealer". Specifically, the plasma force was oriented perpendicular to the camber line in order to resist the leakage flow through the tip gap. Both steady and unsteady forcing was used as a method for manipulating natural jet-like instabilities that existed as the leakage flow separated in the tip gap. The results have indicated that the unsteady plasma forcing was as effective as the passive squealer geometry in reducing the losses that occurred in the wake of the blade tip.

15. SUBJECT TERMS
Plasma actuator, flow control, tip flows, turbomachinery

16. SECURITY CLASSIFICATION OF:			17. LIMITATION OF ABSTRACT	18. NUMBER OF PAGES	19a. NAME OF RESPONSIBLE PERSON
a. REPORT	b. ABSTRACT	c. THIS PAGE			19b. TELEPHONE NUMBER *(Include area code)*
U	U	U	UU	70	

Tip Clearance Control Using Plasma Actuators

Scott C. Morris and Thomas C. Corke

Final Technical Report

by the

University of Notre Dame

Notre Dame, Indiana

for the

Air Force Office of Scientific Research

Contract No. FA9550-04-1-0198

UND-SM07-0328
March 2007

EXECUTIVE SUMMARY

This report documents experimental results from a series of experiments using active flow control to improve the performance and efficiency of turbines. The region of specific interest was the leakage flow that exists between the rotating blades and the endwall in a non-shrouded turbine design. The flow control was based on Single Dielectric Barrier Discharge (SDBD), or "plasma actuators". These actuators are ideal for the harsh turbine environment because they are typically constructed from the same materials currently used in turbine blading, they require only a small electrical supply, and they do not have any moving parts.

Two experimental facilities were used as part of this research project. The first was a low-speed, large-scale turbine cascade using Pak-B turbine blades. The second was a smaller scale, high-speed cascade with low aspect ratio with the same blade section. The measurements included end-wall static pressure, total pressure losses in the wake, blade pressure, and blade-tip flow visualization. These data were acquired over a variety of independent parameters for the baseline geometry, modified tips with passive flow control, and a blade tip which incorporated a plasma actuator.

The active flow control was design to act as a "plasma squealer". Specifically, the plasma force was oriented perpendicular to the camber line in order to resist the leakage flow through the tip gap. Both steady and unsteady forcing was used as a method for manipulating natural jet-like instabilities that existed as the leakage flow separated in the tip gap. The results have indicated that the unsteady plasma forcing was as effective as the passive squealer geometry in reducing the losses that occurred in the wake of the blade tip. It was also found that the thickness of the blade tip, given in terms of the thickness-to-gap ratio, was a dominant variable in controlling the effectiveness of both passive and active control strategies. The mechanisms responsible for these results are postulated in terms of the tip-gap flow topology.

1.0 INTRODUCTION

This report describes the first use of active flow control of the tip clearance region of a linear turbine cascade using plasma actuators. The intent of the active control is to gain overall improvements to a turbine's ability to reliably convert the total enthalpy of the working fluid into useful work. The efficiency of this process depends on flow irreversibilities that occur in the turbine. The over tip leakage flow (OTL) and other secondary flow features are known to be the main contributors to the net losses in axial flow turbines (Xiao et al. (2001) and McCarter et al. (2001)). The working hypothesis of this research is that active, blade mounted flow control actuators will provide a method to reduce or modify these secondary flow features in order to obtain a net benefit to the operation of turbines in propulsion applications.

The tip clearance of a turbine varies around its operation cycle, and increases during the engine life due to wear. The sensitivity to gap clearance is exceedingly important to the turbine design. Active flow control has the potential to both increase optimal performance, and to desensitize the turbine performance from gap clearance. This will become essential in proposed "high-work" turbine designs with fewer stages and higher power-to-weight ratios, where the high blade loading would increase the OTL. With any flow control application, the objective is to identify (or create) a location within the flow field that is sensitive to low levels of actuation. In other words, one wishes to spend a minimum amount of energy in exerting the control, with a benefit that is significant compared to the penalty that is introduce by the actuation mechanism (energy expenditure, extra weight, durability issues, etc.). It is envisioned that an optimal configuration in a rotating machine will result from a blade and casing design that considers both passive and active control mechanisms throughout the machine.

The actuators used in the present experiment were single dielectric barrier discharge plasma actuators (Enloe et al(2004)). The plasma actuators are ideal for the turbine application for a number of reasons. The actuators are small, solid state, electrically driven and can be made to be flush with a solid surface. Because the actuators only require an a.c. voltage for operation, it is possible to use the actuators on the rotating frame, and thus allowing the control actuation to occur directly on the blades where the secondary vorticity is generated. The present effort is focused on actuators mounted near the tip gap of a linear cascade. This builds upon extensive experimental development and numerical modeling of weakly-ionized plasma actuators for flow control

applications. Successful demonstration of these actuators includes leading-edge separation control related to helicopter retreating-blade stall (Corke et al. (2002)), trailing edge separation control in turbine blades for LPT applications (Huang et al (2003)), and control of boundary layer instabilities (Corke and Matlis (2000)).

The flow around a turbine blade - endwall is complex, turbulent, and highly three dimensional. The authority of a specific actuator configuration will depend highly on the placement, actuation level, and sensitivity of the local flow to the input. The purpose of the present set of investigations was to utilize a cantilevered blade in two separate turbine cascade facilities to study the effects of active control in an experimentally "friendly" environment. The existing literature describes this flow field in great detail, and is used to guide the development of the actuators.

The majority of information about the end-wall flow associated with turbine blades comes from studies performed on linear cascades (Papa et al (2003), Wei). Recently detailed measurements have been obtained in a low speed rotating machine (Xiao et al. (2001) and McCarter et al. (2001)). The physical picture of the blade gap-clearance flow that emerges from such studies can be summarized as follows:

1. the flow through the gap between the blade and the casing wall is driven by the pressure difference between the pressure and suction sides of the blade,
2. there is a sharp turning of the flow at the pressure-side corner of the blade leading to a separation bubble that forms on the underside of the blade,
3. there is a sharp flow acceleration forming a vena-contracta under the blade,
4. the leakage flow from the tip-wall gap emerges as a jet on the suction side of the blade,
5. the interaction of the leakage-flow jet with the main flow causes the jet to roll up into a streamwise vortex on the suction side of the blade,
6. the growth and spreading of the tip vortex results in irreversible mixing and loss of work.

The basic physical phenomena summarized suggests a number of possible approaches to minimizing the total losses in the turbine with flow control. First, minimizing the net leakage flow should intuitively reduce the net losses. Of equal importance, is the mixing of the leakage on the suction side of the blade.

One approach is to modify the secondary flows that are causally related to the OTL flow. The effect of the pressure and suction side secondary velocities are quantified by the loss model pro-

posed by Denton (1993). A number of investigators have used partial shrouds, or "winglet" designs to reduce the secondary flow field velocity near the tip (Yaras and Sjolander (1992), Dey (2001), Harvey and Ramsden (2001). It has generally been found that pressure side extensions have a significant effect on the OTL, whereas the suction side extensions have little effect.

A second, and perhaps more direct approach is to minimize the mass flow through the tip gap. The reduction in net leakage is characterized by the discharge coefficient, C_D of the gap. The tip leakage losses can also be modeled in terms of C_D. The effect of blade-end shaping on the tip leakage flow has been studied by several authors. For example, Booth et al. (1983) carried out an extensive investigation of rotor tip geometries that were aimed at reducing the discharge coefficient. Knife-edge, or "squealer" tip blades were found to have 25% lower leakage flow rate compared to plane tip blades. Heyes et al. (1991) found that a single sided squealer on the suction side of the tip was most effective. Key and Arts (2004) compared flow visualization and the pressure field of a flat tip and squealer geometry.

Active flow control has a clear advantage compared to passive techniques because the active control can use an unsteady forcing frequency to excite a naturally occurring instability. For example, Bae et al.(2000) used synthetic jets in a linear compressor cascade and found a reduction in OTL flow. The results were found to be very dependent on the forcing frequency.

It is important to consider that there are two time scales that are associated with the OTL flow. First, the pressure difference across the blade creates a wall jet whose time scale can be derived from the jet velocity and the gap size. Secondly, the tip vortex roll up process occurs at length and time scales that are properly represented by the tip relative velocity and the blade chord length. Although the tip velocity and the wall jet velocity are likely to be of the same order, the tip to chord ratio is often of order 1-3%. Thus, the time scales of actuation that will have the most impact on the wall jet dynamics will be two orders of magnitude different from the time scales of the tip roll up process. The plasma actuators described below are ideal for working with various time scales since the actuation is inherently unsteady due to the a.c. excitation voltage, and the voltage can be amplitude modulated at a desired frequency.

The remainder of this report is outlined as follows. Section 2 presents the basic features of the two linear turbine cascade facilities that were used in this research. The plasma actuators are described

in Section 3, including a basic explanation of the physics of the actuators as well as the blade-tip actuator design. Sections 4 through 7 present results from the various experimental programs that were conducted as part of this project. An overall summary including the main conclusions that can be taken from the results are given in Section 8.

2.0 EXPERIMENTAL FACILITIES

The experiments described in this report were conducted in two separate linear cascade facilities. These are described in the following subsections.

2.1 Large Scale Pak-B cascade facility

The tip clearance leakage was investigated in a large-scale, low-pressure linear turbine cascade located in the Hessert Laboratory at the University of Notre Dame. Nine generic "Pak-B" blades designed by Pratt & Whitney were installed as a cascade blade array, of which five can be seen in Figures 1 and 2. Here, flow is from left to right. The tip clearance gap is located on the near end adjacent to the clear Lexan endwall. The blades have an axial chord of 15.95 cm, a span of 0.91 m, and a turning angle of 95 degrees. The Reynolds number, based on inlet freestream velocity and axial chord, was able to be varied between 10^4 and 10^5. The stagger angle is 26.16 degrees and the pitch spacing is 14.12 cm. These values give a solidity of 1.13. Two tailboards were used, one at each of the outer two most blades in the array, to match the pressure distribution in the cascade to an inviscid Euler numerical simulation. The center most blade has a variable gap-to-chord ratio (τ/c) ranging from zero to five percent, which can be altered by shimming the blade fixed end. This center blade will be referred to as the "test blade" in all cases. The blades immediately adjacent to the test blade are cantilevered with a nominal tip gap of 1.25 percent of chord, to simulate semi-realistic periodic boundary conditions. In the experiments, the effect of Reynolds number and tip gap spacing on active flow control effectiveness were investigated in detail.

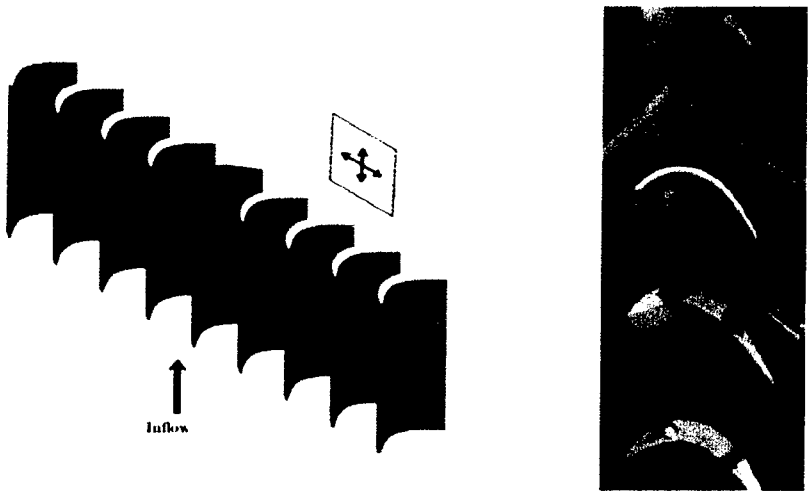

Figure 1 Schematic and Image of large scale linear cascade arrangement.

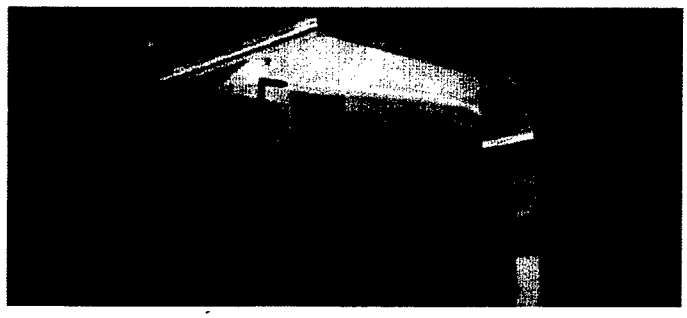

Figure 2 Image of test blade with 5 hole probe mounted downstream of the open tip gap

2.2 High speed Pak-B cascade facility

A new facility was designed and constructed as part of this project in order to obtain active flow control measurements at higher Mach number. A schematic and photograph of the facility are shown in Figure 3. All measurements were conduced at Reynolds numbers from 100,000 to 500,000 based on the inlet velocity. The inlet and exit Mach numbers were 0.2 and 0.3, respectively at Re=500,000. The setup was a three blade (two passage) linear cascade comprised of a Pratt & Whitney Pak-B low pressure turbine blade shape. The stagger angle of the blades was 26.2 degrees. The blade chord, c, was 4.61 inches, with a corresponding axial chord, c_x of 4.14 inches. The span was 4 inches. The solidity was 1.13. The outer two blades spanned the entire

cascade and intersected the tunnel walls at both spanwise locations. The middle blade was instrumented and cantilevered from the inside wall leaving a small tip clearance from the outside endwall. Removable plastic shim spacers shaped like the blade profile were added to the center blade to provide different gap spacings. The shims permitted gap sizes of up to 8.0 percent of c_x. All three blades were cast in a two-part epoxy from a numerically machined mold.

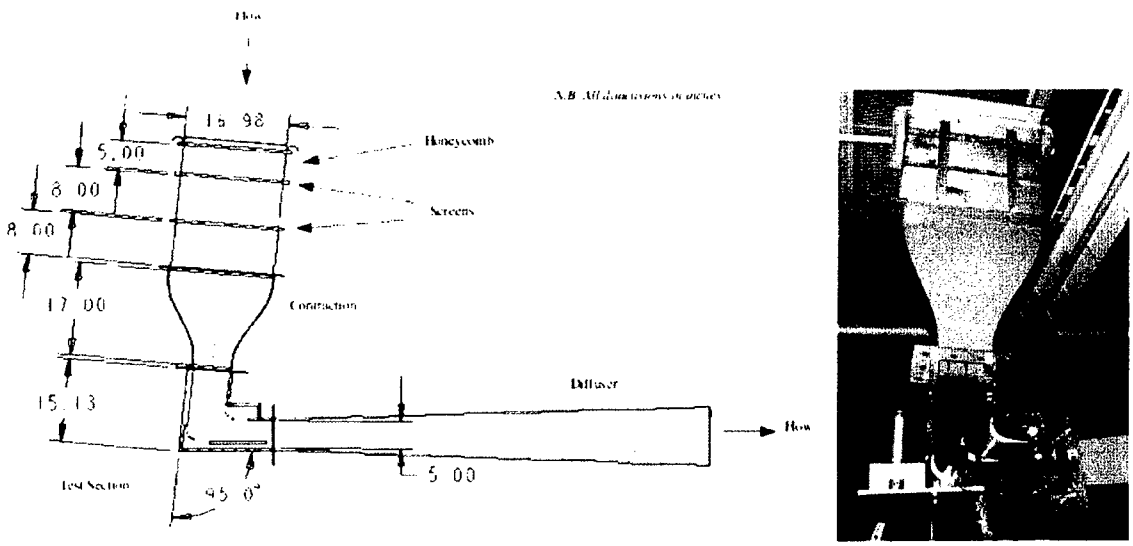

(a) Wind Tunnel (b) Test Section

Figure 3 Schematic and Image of the high speed linear cascade facility

3.0 PLASMA ACTUATOR DESIGN

3.1 Basics of the SDBD actuator

Plasma enhanced aerodynamics has been demonstrated in a range of applications involving separation control, lift enhancement, drag reduction and flight control without moving surfaces (Post (2003), Huang et al. (2003), Post (2004), He et al. (2004), Corke et al. (2004, 2006). The fundamental components for this "plasma actuators". The plasma actuator consists of two electrodes that are separated by a dielectric material. One of the electrodes is exposed to the air. The other electrode is fully covered by the dielectric material. A schematic illustration of the actuator configuration used in the cited applications is shown in Figure 4. A high voltage alternating current (a.c.) input is supplied to the electrodes. When the a.c. voltage amplitude is large enough, the air ionizes in the region of the largest electric potential. This generally begins at the edge of the electrode that is exposed to the air, and spreads out over the area projected by the covered electrode. The location of the plasma is denoted in Figure 4.

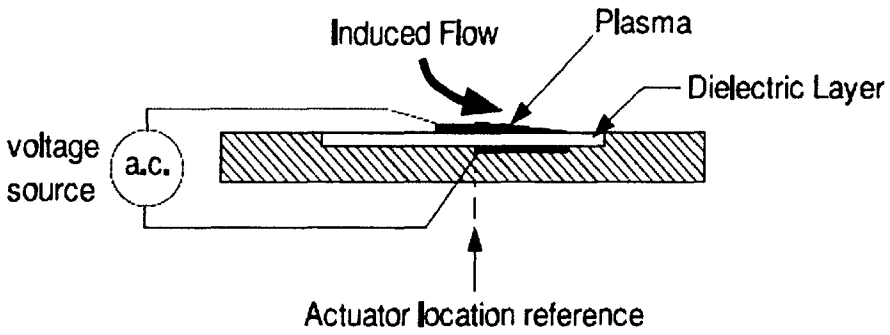

Figure 4 Schematic drawing of SDBD plasma actuator illustrating asymmetric electrode arrangement, dielectric layer, and location of plasma formation. The actuator location is referenced to the junction of the exposed and covered electrodes

The process of ionizing the air in this configuration is classically known as a single dielectric barrier discharge (SDBD), (see Enloe et al. 2003). It has the property that it is self-limiting and therefore stable at atmospheric pressures. During the a.c. cycle, the electrons and ions move according to the sign in the alternating electric potential. As they move, the surface of the dielectric becomes charged. When the potential difference between the exposed electrode and the dielectric surface is large enough, the air over the dielectric layer ionizes. This continues until the charge on the dielectric surface builds up to the point that the potential difference is below the threshold for ionization and the process stops. This is the self-limiting aspect of the dielectric barrier that prevents

a cascade of charges that would cause an electric arc, and distinguishes it from other approaches that use an air gap between uncovered electrodes. With the SDBD approach there is minimal heating of the air, and temperature change is not the mechanism for flow control. A key element in improving the performance of the SDBD plasma actuators is understanding and modeling the dynamic process in which the air ionized during the a.c. cycle, (Orlov (2006)). The method of solution to obtain the body force starts with a lumped-element model which determines the space-time distribution of charge on the surface of the dielectric. This sets the time dependent boundary conditions on the electric potential on the dielectric, $\varphi_s(x)$, that are used in solving the electrostatic equation for the electric potential in the spatial domain. The electric field, $\vec{E}$, is then found from the solution of Laplace's equation. The body force vector is determined from the body force equation:

$$\vec{f}_b = \rho_c \vec{E} = -\left(\frac{\varepsilon_0}{\lambda_D^2}\right) \varphi \vec{E}. \tag{1}$$

The plasma actuator body force vector can be tailored through the design of the electrode arrangement and the dielectric material, which control the spatial electric field. The body force representation is also a convenient form to incorporate the effect of the actuators in Navier-Stokes (N-S) simulations of the flow field. Such N-S simulations have been used to design and optimize different plasma actuator arrangements (Orlov (2003), Orlov (2002), Orlov (2004)). Another actuator optimization comes from the choice of the a.c. time series shape, which controls the duration and extent of the plasma.

In flow simulations, the body force enters the governing equations for the flow in the momentum equation. This implies that the effect of multiple actuators has an additive effect on the momentum. Post (2004) performed experiments to investigate this. Results of this are shown in Figure 5. This involved measuring mean velocity profiles of the actuator-induced flow at a fixed distance from a series arrangement of SDBD plasma actuators having the asymmetric electrode design shown in Figure 4. The asymmetric electrode design results in a body force that induces the flow in the direction from the exposed electrode towards the covered electrode (see arrow in Figure 4). This produces a wall-normal mean velocity distribution that is similar to a tangential wall jet. The left plot in Figure 5 documents examples of the profile shape. Each symbol corresponds to separate measured profiles. The number before the "A" in the label indicates the number of actuators

being operated at one time (1,2 or 3) in this figure. Profiles like these were integrated in the wall-normal direction to determine the momentum produced by the actuators. This has been normalized by the momentum with one actuator operating. The symbols labeled "*Higher* V_{app}" correspond to the profiles that were presented in the left part of the figure. The other symbols were at a lower applied voltage and investigated up to five series actuators. Since the actuator effect acts as a body force, we expect that the induced momentum would be linear with the number of actuators. The dashed line indicates that trend. It appears that the data approximate that behavior, especially when two to five actuators are operating. This summing effect of the plasma actuator supports the body force model, and points to an approach for improving its effectiveness in high-speed applications.

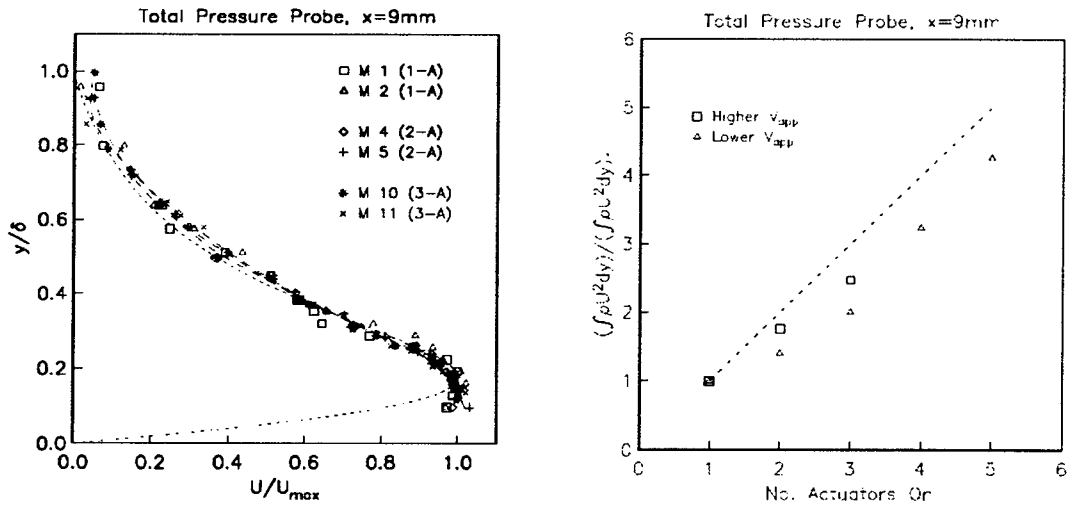

Figure 5 Normalized mean velocity profiles (left) and normalized momentum (right) of the actuator-induced flow for different numbers of SDBD plasma actuators arranged in series. From Post (2004).

Post (2004) has shown that the peak velocity in profiles like those in Figure 5 for a single actuator, varies as $V_{app}^{7/2}$. Enloe et al.(2003) observed the same dependence on thrust produced by a SDBD plasma actuator. The flow simulations that include the plasma actuator model have shown excellent agreement with experiments on leading-edge separation control in both steady and unsteady cases. This gives us confidence in using the flow simulations to design plasma actuator configurations that are aimed at a variety of flow control situations including the flow in the tip-gap region of the turbine-blade cascade.

3.2 Plasma "Squealer" Design

A significant advantage of the plasma actuator is the ability to configure a distributed thrust vector to accomplish a specific effect. The turbine tip gap flow field, despite its complexity, has a number of known features that guided the initial development of tip gap flow control. Two images of the actuator design are shown in Figure 6. The actuators were incorporated into a dielectric material that was machined to the Pak-B blade shape. These actuators were fixed to the end of the cantilevered blade section. Thin copper strips were secured to the blade surface to connect the actuator electrodes to the high voltage power supply.

The lower (unexposed) electrode was configured to cover the majority of the blade cross section. the upper electrode was positioned near the suction surface as shown in Figure 6. The resulting body force was nominally perpendicular to the local blade camber line. The intent of this design was to simulate the aerodynamic benefits of a squealer tip geometry. Specifically, the squealer tip is known to reduce the discharge coefficient of the tip gap, thereby reducing the mass flux through the tip. The "plasma squealer" was intended to have a similar effect through a number of possible mechanisms. First, the time average of the plasma thrust vector provides additional turning of the main fluid. That is, the plasma tends to aerodynamical fill the gap. Note that this force, although small, would add to the net work output of a rotating turbine. A second potential operating mechanism of the plasma squealer is to provide an unsteady excitation of the gap fluid. Specifically, the separating and re-attaching flow that exists in the tip gap could be excited to produce a localized region of intense mixing and blockage. This would also result in a net reduction of the mass flow through the gap, thereby increasing the net efficiency. The following sections describe results from experiments which have incorporated the plasma squealer into the tip geometry

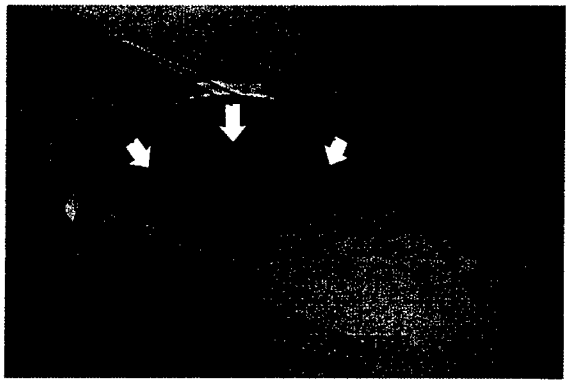

(a) Actuator Design with Resultant Body Force

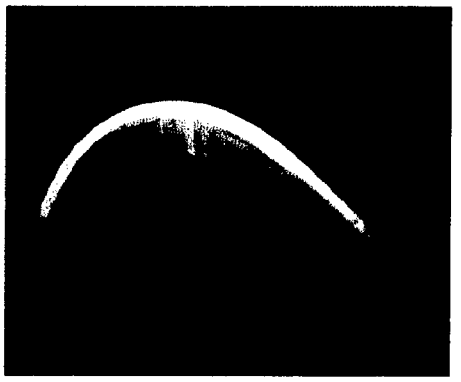

(b) Mounted Blade Tip Actuator

Figure 6 Images of the actuator configured as a "plasma squealer"

4.0 FIRST CONTROL RESULTS - LOW SPEED CASCADE

4.1 Measurement Technique

It is important to be able to accurately quantify changes in the tip leakage flow and resulting tip leakage and passage vortex motions. Because of the small gap sizes presented here, flow measurements were restricted to gap flow wake surveys. The vortices were studied using a 3.175 mm diameter five-hole probe from United Sensor Corporation, located downstream of the cascade blade array. This probe was useful in acquiring mean velocity and pressure readings over a grid of points within the flow field. The probe was completely immersed in the flow and featured a cobra type conical shaped head. This configuration allowed for measurements to be taken close to the blade endwall. An image of the probe located downstream from the blade array is shown in Figure 2.

Ensemble averaged mean pressure readings were taken for the five probe ports, the upstream dynamic pressure from a wall mounted Pitot-static tube, and the downstream endwall static pressure using a Validyne DP103 variable reluctance transducer with interchangeable metal diaphragm. A forty-eight port Scanivalve pressure multiplexer allowed the transducer to scan each port successively for a specified point in the flow field. The probe was traversed in the spanwise and pitchwise directions over a spatial grid of points in a two dimensional plane downstream of the cascade blade array oriented parallel to the blade array trailing edge plane. A representation of this measurement plane in relation to the cascade array is illustrated in Figure 1.

The distance of the measurement plane downstream of the test blade was varied from x/c = 1.25 to x/c = 2.2 to observe the spatial evolution of the tip leakage and passage vortices. Here, x/c = 0 corresponds to the test blade leading edge, x/c = 1 corresponds to the test blade trailing edge, and c is the axial blade chord. Both vortices were fully captured by adjusting the spanwise and pitchwise dimensions for each measurement plane considered.

The acquisition of pressure and velocity at a number of equally spaced points in the flow field allowed streamwise vorticity and pressure loss coefficient contours to be computed. Streamwise axial vorticity was determined from the local velocity vectors as:

$$\Omega_x = \frac{\partial w}{\partial y} - \frac{\partial v}{\partial z} \tag{2}$$

Here, w and z are the Spanwise velocity and direction, respectively, while v and y are the Pitch-wise velocity and direction, respectively. It should be noted that in the coordinate system used, a positive streamwise vorticity is counterclockwise. The pressure loss coefficient is defined [Denton, 1993] as the change in total pressure between the upstream (inlet) and local downstream (exit) values, divided by the local downstream dynamic pressure:

$$C_p = \frac{P_{t_i} - P_{t_e}}{P_{t_e} - P_e} \tag{3}$$

(4)

(5)

The local downstream static pressure was taken as the average of the four probe static pressures. In addition to vorticity and pressure loss coefficients, the identification of vortices was also performed through the use of the λ_2 criterion, as given in the paper by Jeong and Hussain (1995). This method consistently identifies a vortex as the region of negative eigenvalues within a two-dimensional measurement plane.

4.2 Five-Hole Probe Calibration

The five-hole probe was calibrated at a Reynolds number of 5×10^4 and traversed in the blade wake to find local pressure and velocity using a calibration method developed by Bryer and Pankhurst [Bryer and Pankhurst (1971)]. Calibration consisted of yawing and pitching the probe over a large range of pitch (α) and yaw (β) angles in a known one-dimensional flow field and recording all five port pressures for each combination of pitch and yaw angle. A calibration map which correlates the pitch and yaw angles to the change in port pressures was then created, as seen in Figure 7.

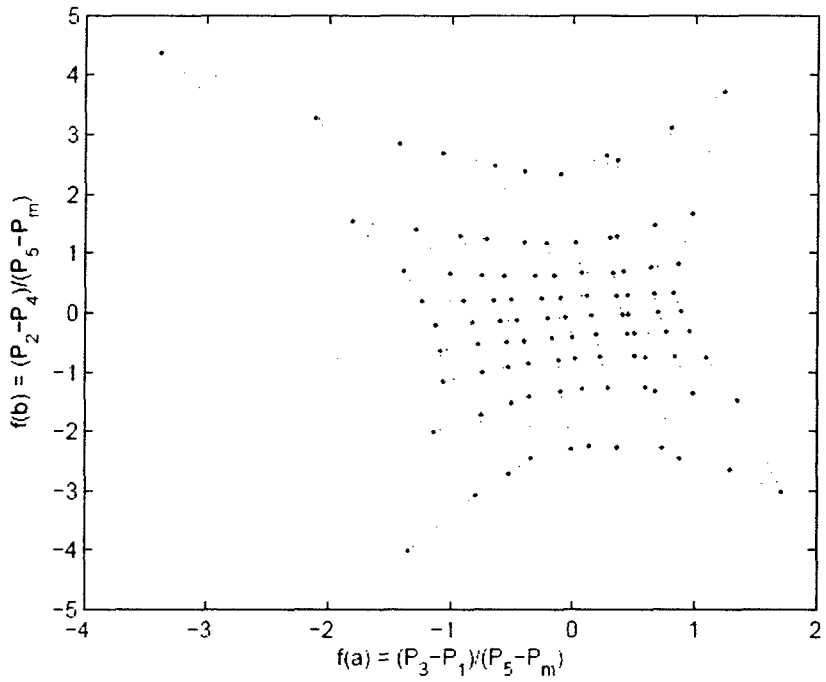

Figure 7 Five-hole Probe Calibration map for $f(\alpha)$ vs $f(\beta)$.

Each dot on this map corresponds to one calibration point, and the lines connecting each dot are lines of constant α or constant β. The functions of α and β that relate the angles to the port pressures are given by

$$f(\alpha) = \frac{P_3 - P_1}{P_5 - P_m} \tag{6}$$

$$f(\beta) = \frac{P_2 - P_4}{P_5 - P_m} \tag{7}$$

Here, subscripts '1' and '3' represent the lower and upper static ports on the probe, while '2' and '4' represent the two side static ports on the probe. Subscript '5' denotes the total pressure port on the probe, and subscript *m* is the average of all four static ports on the probe. When the probe is subjected to an unknown flow velocity at an unknown angle, the flow point on this calibration map, found from the port pressures, will yield the respective flow vector for this unknown flow.

A limitation of the probe was found for the tip leakage vortex surveyed at a large tip clearance gap of 4% axial blade chord. It is known that the tip leakage vortex grows with increasing gap size. At this gap height, because of the large pitchwise and spanwise components of the flow vectors within part of the tip leakage vortex, the port pressures lie far outside the range of pitch and yaw

angles that the probe was calibrated for. This means that the probe will unable to resolve the flow field for part of the tip leakage vortex at a clearance of 4% or greater. To correct this limitation, the probe was calibrated for greater flow angles. Unfortunately, at large pitch and yaw angles, the flow on the probe appeared to separate, causing calibration points for these angles to be unreliable. Still, the range over which the calibration points were well-behaved was quite extensive, with α having a range over [-25,25] degrees and β over [-38,34] degrees.

This phenomena was found for a number of downstream measurement planes at a 4% gap for $Re_c=10^5$. For planes ranging from x/c = 1.25% to x/c = 2.2%, Figure 8 shows the flow points, represented as blue crosses, for the tip leakage vortex as they are plotted over the calibration map. At one-quarter axial chord downstream from the trailing edge, the tip leakage vortex is the strongest of all the plots, and the flow points deviate the most from the calibration region. As the probe is moved farther away from the trailing edge, the flow points move closer and eventually within the calibrated region.

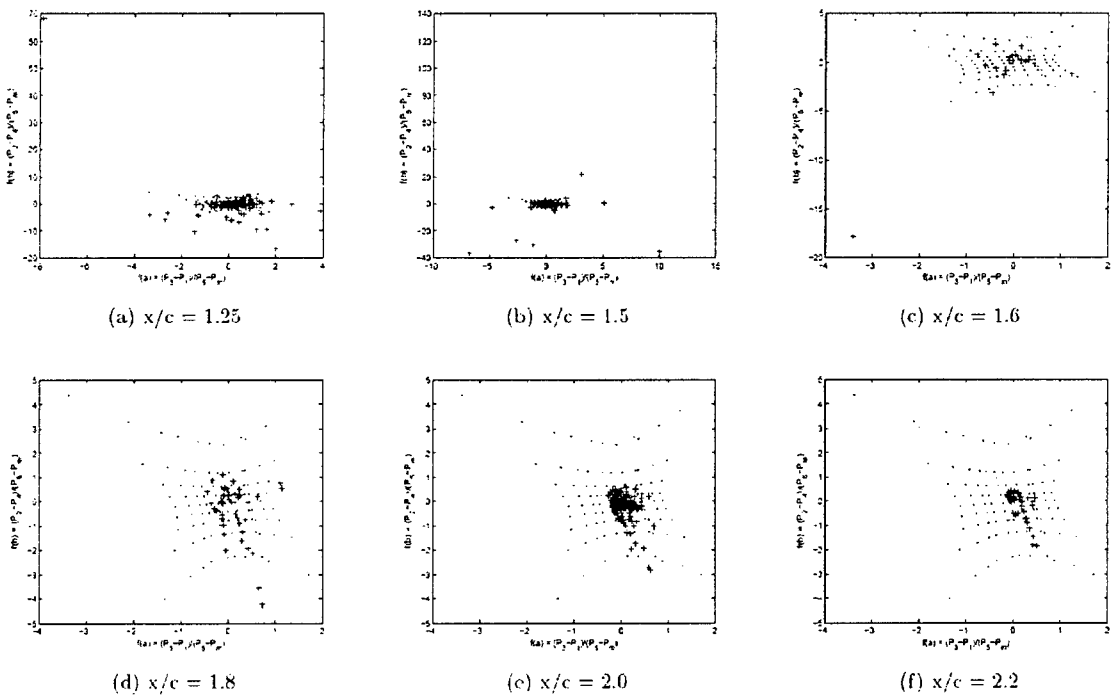

Figure 8 Calibration scatter plots for varying downstream distances at $Re_c=10^5$, $\tau/c=4$.

It should be stated that the problem is independent of the specific calibration or probe used here. This problem is a limitation in the measurement technique of using multi-hole probes in low Reynolds number blade tip flow surveys that has not been reported previously.

The problem with the inability to resolve the part of the tip leakage vortex with the largest flow angles is that this region contains the strongest negative vorticity and the highest losses in the tip region flow field. The maximum loss coefficient will be undetectable, and so a change in loss coefficient will be unable to be quantified accurately here. Also, because the flow vectors are not able to be determined, neither streamwise vorticity contours nor the λ_2 criterion will be able to be found.

To help circumvent this problem, it is helpful to remember that the tip leakage vortex scales with gap height. Reducing the gap will decrease the mass flow through the gap, and lessen the maximum flow angles and streamwise vorticity magnitude. So, to capture the entire flow field, the tip gap was reduced to $\tau/c = 1.56$. At this gap height, all flow vectors were found to fall well within the calibrated region for the probe. This gap height allowed a fair and accurate comparison of the tip leakage vortex for varying downstream axial planes both with and without active flow control.

4.3 Active Flow Control Optimization and Results

The improvement in efficiency near the blade tip is dependent on the mechanism of flow actuation. Here, the driving frequency of the plasma actuator can affect instabilities that are present within the tip gap flow field. The measure of efficiency increase is gauged by the amount of total pressure increase in the downstream wake of the blade array. In an adiabatic stage, entropy production is caused by a decrease in total pressure through the stage. To find the frequency dependence of the tip flow field, a sensitive point in the downstream wake is chosen and the total pressure is acquired for a range of frequencies. A point is typically chosen at the edges of either the leakage or passage vortex because changes in total pressure in these regions will easily indicate a change in vortex size or strength with frequency. At $Re_c=10^5$ and $x/c=1.5$ for the small gap of $\tau/c = 1.56$, the percent change in total pressure from the unactuated case is plotted against the nondimensional actuation frequency in Figure 9. Here, lines are drawn for visual reference only.

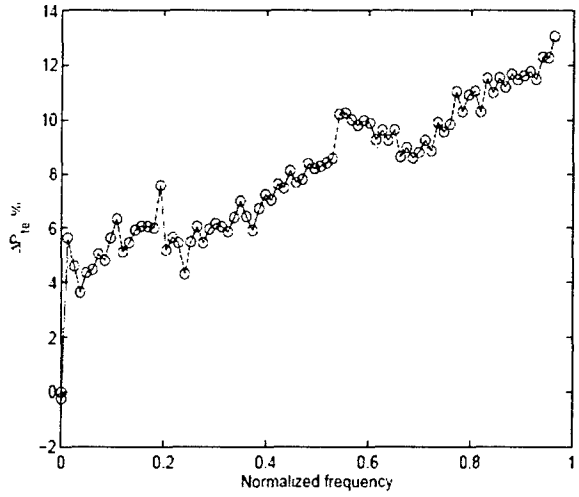

Figure 9 Frequency Dependence of downstream total pressure at z/c=0.12, x/c=1.5.

At $Re_c = 10^5$, at this point in the flow field, there is a monotonic increase in downstream total pressure, and therefore, efficiency. A nondimensional frequency of zero denotes the unactuated case. Taking a high frequency of $f = 0.8$ where a significant change in total pressure is seen, unactuated and actuated surveys were performed at x/c = 1.5. This nondimensional frequency corresponds to an actuation frequency of 3.3 kHz.

The unactuated and actuated vorticity contours are plotted in Figure 10. Overlaying the vorticity contours are the *v* and *w* component velocity vectors as well as the λ_2 criterion which outlines a vortex. The view shown looks upstream toward the blade array on the suction side passage of the test blade. The cascade endwall is represented by a horizontal black line at the top of the vorticity plots. The trailing edge suction side edge of the test blade is represented by a vertical black bar at y/p = 0.725. The tip leakage vortex is highlighted as a region of negative vorticity around y/p = 1.05, z/c = 0.033. The passage vortex is a larger region of positive vorticity located at y/p=1.15, z/c = 0.2. The horseshoe vortex is also visible at y/p = 0.9, z/c = 0.4.

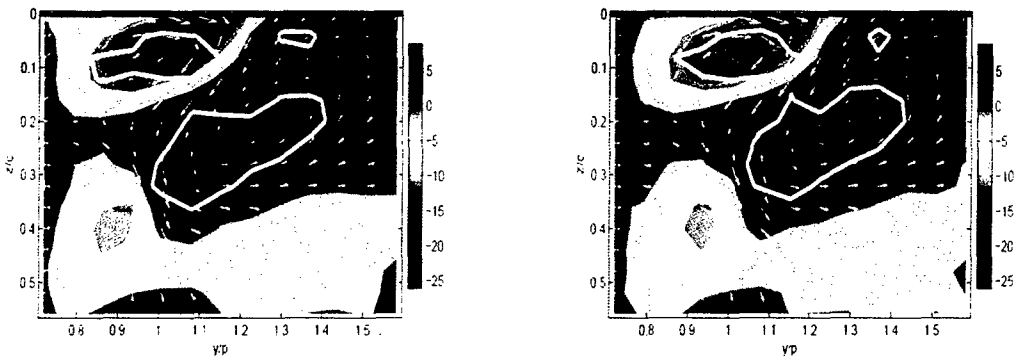

(a) Unactuated Case (b) Actuated Case for f = 0.8

Figure 10 Streamwise axial vorticity for x/c=1.5, τ/c=1.56, and $Re_c=10^5$.

With actuation, the three vortices present all move away from the suction side blade surface. The maximum extent of the tip leakage vorticity is seen to decrease slightly, based on the size of the maximum negative vorticity and the size of the λ_2 surrounding it. The passage vortex seems to be unaffected, while the horseshoe vortex decreases in size but increases in strength.

It is also helpful to examine contours of pressure loss coefficient, which are displayed with and without actuation in Figure 11. Here, the lines representing the test blade and endwall locations are displayed in red instead of black for clarity against the darker pressure coefficient contours. With actuation, the maximum pressure loss coefficient in the tip leakage vortex decreases by 29.5% over the unactuated case. Also, the passage vortex and tip leakage vortex have a greater interaction with actuation. Overall, for $Re_c = 10^5$, the plasma actuator has a substantial effect on the leakage flow.

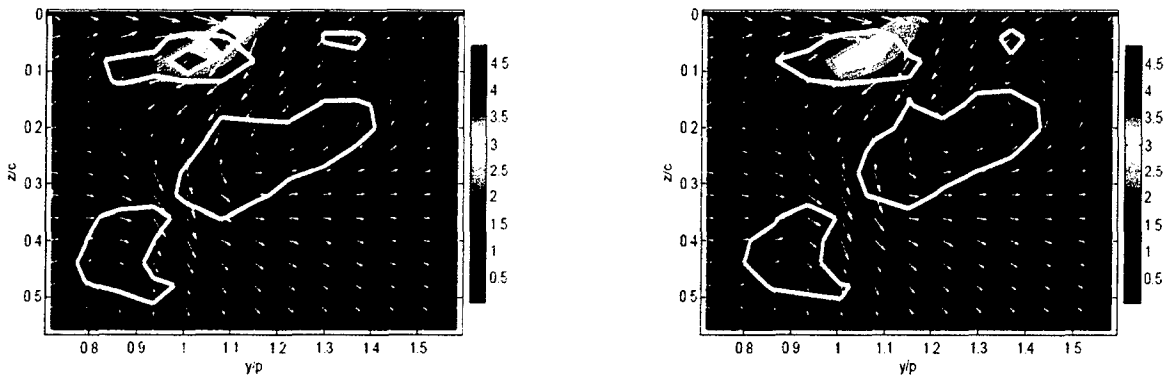

(a) Unactuated Case (b) Actuated Case for f = 0.8

Figure 11 Pressure loss coefficient for x/c=1.5, τ/c=1.56.

To see the Reynolds number dependence on actuation, the actuator optimization above was repeated at $Re_c = 5x10^4$. The frequency dependence of the flow field was examined again for x/c= 1.5 and τ/c = 1.56, now at y/p = 1.08, z/c = 0.08, which corresponds to the edge of the tip leakage vortex at this lower Reynolds number. Here, the flow exhibited a clear optimal dependence on actuation, with a maximum improvement around f= 1.6, as seen in Figure 12. This nondimensional frequency corresponds to an actuation frequency of 3.3 kHz. In this plot, the percent change in downstream total pressure is significant, because the unactuated pressure is very low here. It is thought that even a slight change in the magnitude or location of the tip leakage vortex would cause a significant change at the point surveyed here.

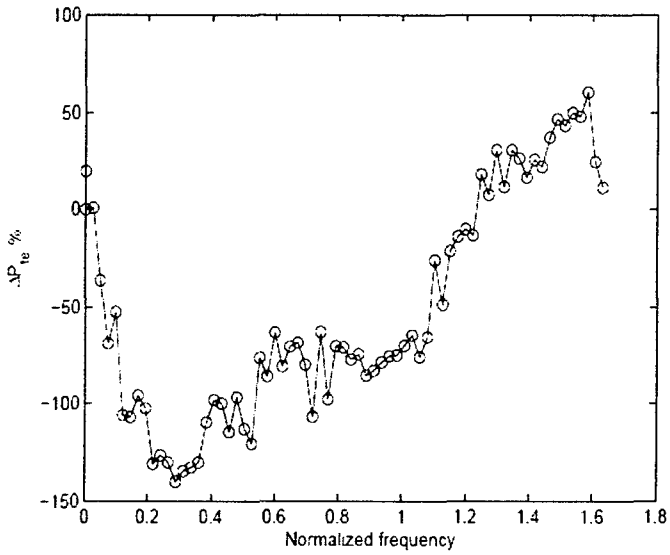

Figure 12 Frequency dependence of downstream total pressure at Re_c=5x10^4.

Examining the streamwise vorticity contours with actuation in Figure 13, the size of the vorticity in the tip leakage and passage vortices increases. Again, the small shift toward the pressure side of the adjacent blade from the test blade is seen here, as with the $Re_c = 10^5$ case.

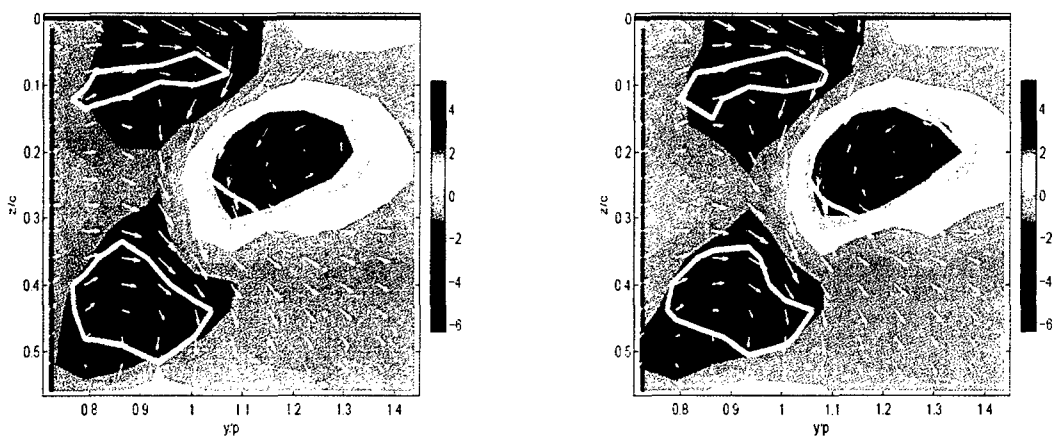

(a) Unactuated Case (b) Actuated Case for f = 1.6

Figure 13 Streamwise vorticity for x/c=1.5, τ/x=1.56, Re_c=5x10^4.

Looking at pressure loss coefficients in Figure 14 for the unactuated and actuated cases, the regions of loss for the tip leakage vortex and passage vortex decrease with actuation. It is also noticeable that the maximum loss decreases by 14.7% with actuation in the tip leakage vortex.

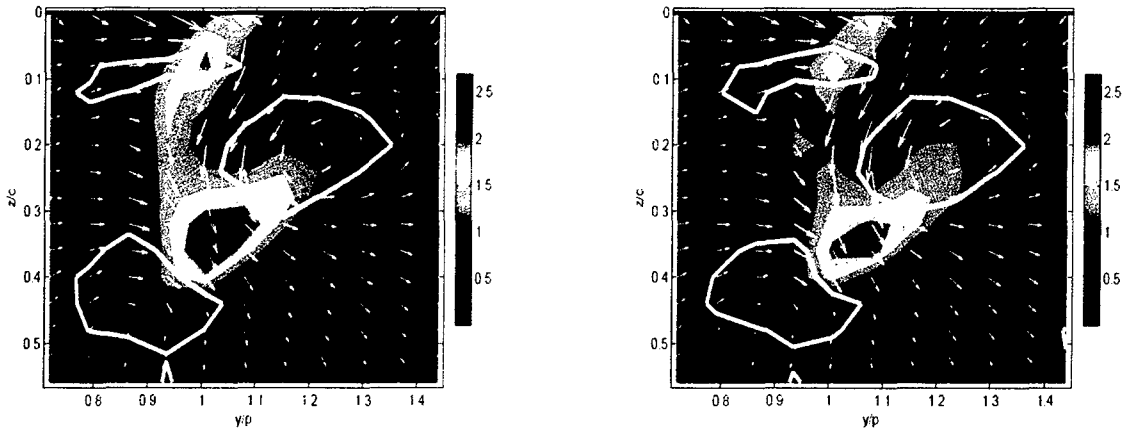

(a) Unactuated Case (b) Actuated Case for f = 0.8

Figure 14 Pressure loss coefficient for Re_c=5x10^4, x/c=1.5, τ/c=1.56.

In the case for $Re_c = 10^5$, the change in downstream total pressure did not experience an optimum, as in the $Re_c = 5x10^4$ case. Although both Reynolds numbers displayed a noteworthy change in pressure loss coefficient, a frequency optimum with Reynolds number should be investigated at higher frequencies for the higher Reynolds number case. Regardless, the effect on the flow field with actuation is promising.

4.4 Conclusions

The use of active flow control has shown a beneficial change in the downstream wake in the blade tip region in a low pressure linear turbine cascade for Reynolds numbers of 10^5 and $5x10^4$ at a tip gap height of 1.56%. Changes in the location of the vortex structures is seen with vorticity contours and a λ_2 criterion for both Reynolds numbers. Improvement in the maximum value of loss coefficient for both Reynolds numbers was also found. The loss coefficient improvement for $Re_c = 10^5$ showed roughly a 100% increase over the case at $Re_c = 5x10^4$.

For a larger gap of 4%, the five-hole probe was unable to resolve the tip vortex flow field due to high flow angularity in the tip region. The limitation in using a five-hole probe in the wake of the tip leakage vortex, while troublesome, illustrates the large three-dimensional nature of the flow in the blade tip region. The present findings illustrate the need that experiments to follow will require the use of a nonintrusive method, such as Stereo PIV, that can resolve the flow features at larger gap sizes. Reynolds number and gap size dependence will continue to be studied, and future work will also focus on determining the frequency dependence of actuation on the flow improvement.

5.0 COMPARISON WITH PASSIVE CONTROL - HIGH SPEED CASCADE

In order to further the understanding of turbine tip leakage and passage flow mechanisms for undesirable entropy production, an experiment was conducted in a linear cascade at the Hessert Laboratory. Blade surface and tip endwall static pressure, total pressure loss, and wake vorticity measurements were taken to document the effects of upstream axial Reynolds number, $1.0\text{x}10^5 < Re < 5.0\text{x}10^5$, and tip gap height, $0.015 < g/c < 0.08$ for flat and partial, suction-side squealer tip geometries, as well as active flow control using a plasma actuator situated on the blade tip. Interaction of tip leakage and passage vortices proved critical, and an inverse relationship was observed between the two structures in terms of streamwise vorticity, core total pressure loss, and the vortex size denoted by the λ_2 criteria. When a squealer tip is added, the results indicate an effective reduction in gap size, and thus a reduction in loss. However, the high loss region in the gap disappears, indicating that the squealer traps the air in the region. When a plasma actuator is used to control the flow, the effect depends strongly on the unsteady frequency at which it is run. An effect is seen in the downstream loss, however the high loss region in the gap appears unaffected, indicating that this method does not trap air in the tip gap.

5.1 Experimental Procedure

This experimental investigation was conducted in the high speed linear cascade described in Section 2. The middle blade was instrumented and cantilevered with a small tip clearance from the nearby endwall for close investigation of the flow physics. Shim stock spacers permitted gap sizes from 0.5 to 5.0% axial chord. For passive flow control measurements the center blade was outfitted with a partial, suction-side squealer tip measuring 2.5% axial chord in height and covering approximately 75% of the blade suction surface, as pictured in Figure 15.

Figure 15 Image of Pak-B blade tip showing the partial suction-side squealer tip

By drilling shallow holes in an aluminum casting mold and inserting threads of 0.020-inch 0.D. tygon tubing, the middle blade was cast with 15 static taps uniformly dispersed over both the pressure and suction sides of the blade, at midspan and tip spanwise locations. Static pressure coefficients were defined as,

$$c_p = \frac{P_s - P_2}{P_{t2} - P_2}. \tag{8}$$

where P_s, P_{t2}, and P_2 are the local static pressure, upstream total pressure, and upstream static pressure, respectively. Integrating the coefficients yielded a measure of blade loading, deemed $c_{p,blade}$.

In addition, thirty wall static taps were superimposed in ten rows of three over the PakB geometry on the gap-side test section endwall, as depicted in Figure 16. Major differences in flow structure passing "under" the blade through the gap region could be observed with these static pressure measurements. Static pressure coefficients were also defined by Equation 7.

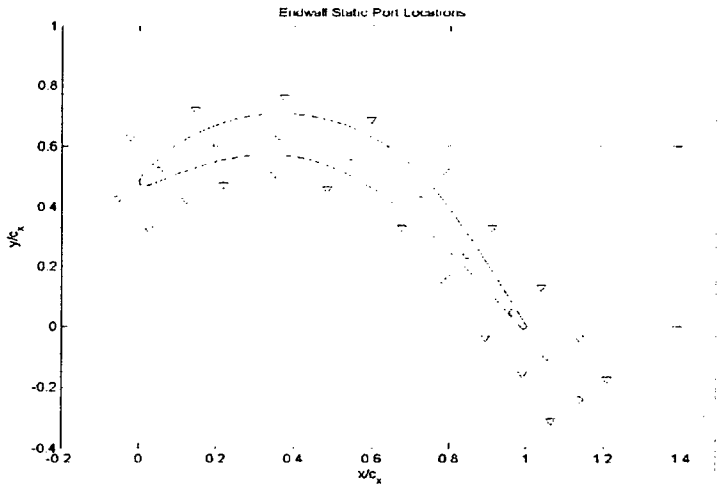

Figure 16 Endwall static pressure tap locations

Lastly, a United Sensor 1/8" five-hole Pitot probe was positioned at 100 points in a 2" by 1.25" (10 by 10) grid by a two-dimensional traverse system. Depicted in Figure 17, tip flow field surveys encompassed approximately one half of a pitch away from the trailing edge and one third of the span from the tip endwall. At each grid location, a total pressure upstream of the blade, the five pressure readings from the five-hole probe, and one downstream static pressure reading acquired from the endwall static taps were referenced against upstream static pressure and recorded to provide point-to-point three-dimensional velocity vectors.

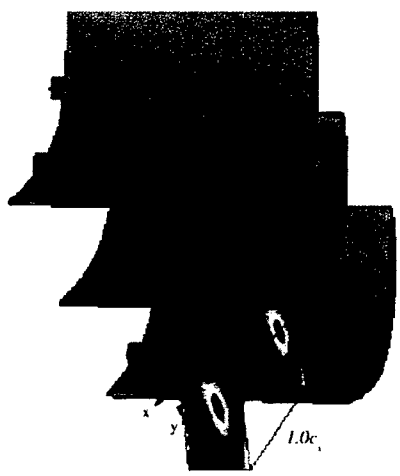

Figure 17 Interrogation Window for 5-hole probe in the wake

A slot was milled in the hub endwall to permit insertion and positioning of the probe body. To prevent the induction of a wall jet due to the high pressure gradient applied across the milled slot, a Lexan box was constructed to hermetically seal the entire traverse assembly and thus eliminate the pressure gradient across it. Further, blade static pressure taps and electrical connections to control the traverse had to be taken outside of the box. An ITT Cannon MIL-C-26482 box-mounting miniature electrical connector linked the motor controllers to the traverse motors located inside of the box, and was specified to leak less than 0.001 cubic feet per hour under a 100 psi differential pressure gradient. Steel tubing was wedged through small, drilled holes through the Lexan walls to bring all of the tygon tubing lines outside of the box. Through the use Lexan walls, silicon sealant, and reinforcing Lexan blocks welded to the original box walls, the entire box assembly was structurally supported and ensured air tight to guarantee an equalized pressure gradient on both sides of the slot.

Reynolds numbers of $1.0\text{x}10^5$, $2.0\text{x}10^5$, $3.0\text{x}10^5$, $4.0\text{x}10^5$, and $5.0\text{x}10^5$ and gap sizes of g/c = 1.5, 4.0 and 5.0% were investigated for baseline, flat tip, and controlled, squealer tip, cases. Table 1 presents the test case matrix for the gap setting of 4% axial chord. Additional gap settings focused on only the extreme Reynolds numbers. For a more thorough discussion of the complete data set, the reader is referred to Douville (2005). Additionally, Reynolds numbers of $2.0\text{x}10^5$ and $5.0\text{x}10^5$ and gap sizes of g/c = 4.0 and 5.0% where investigated for baseline, and plasma actuated cases at a range of frequencies.

Table 1. Structure of the Data Set, $g/c_x = 0.04$

$Re(\times 10^3)$	Squealer Tip	Midspan c_p	Tip c_p	Endwall c_p	Wake Survey
100	√	√	√	√	√
100		√	√	√	√
200	√	√	√	√	√
200		√	√	√	√
300	√	√	√	√	√
300		√	√	√	√
400	√	√	√	√	√
400		√	√	√	√
500	√	√	√	√	√
500		√	√	√	√

5.2 Baseline Results

Pressure distributions of the low aspect ratio blades revealed a highly three-dimensional nature of the passage flow, and as such failed to match a two-dimensional Euler distribution. Instead, the gap was filled with rubber spacers and a distribution was taken at midspan to provide a benchmark from which to qualitatively evaluate effects of gap height, Reynolds number, and tip geometry on the blade pressure distributions. Both midspan and tip pressure distributions varied substantially throughout the data set, so the midspan pressure distribution without gap shown in Figure 18 is the least three-dimensional view of the loading on the PakB blade. Further, because midspan pressure distributions showed similar sensitivity to the change in the parameters and given the proximity of the tip static taps to the gap, distributions presented below are restricted to the more interesting tip cases.

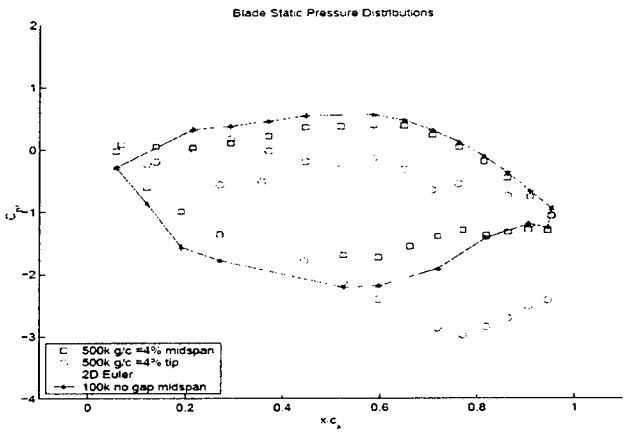

Figure 18 C_p distributions at mid-span and tip locations for g/x=0.04 and Re=5.0x10^5. The dashed curve is the 2-D Euler solution, the solid curve is the midspan distribution at Re=1.0x10^5.

Tip loading was generally lower than that at the midspan due to high spanwise velocities into the gap on the pressure surface. Shown in Figure 19, low speed, Re = 1.0x10^5, blade loading also dropped roughly 25% over the gaps surveyed, but the high speed, Re = 5.0x10^5, loading dropped slightly less at 18.5%. However, the magnitude of the loss in blade loading was nearly equivalent in both cases. Blade loading dropped equivalently for both spanwise locations, which speaks to the highly three dimensional flow at even the midspan. Reduced blade loading over at least half of the span highlights the loss of work input to the turbine due to flow escaping the blade through the tip gap as one of the undesirable tip leakage contributions.

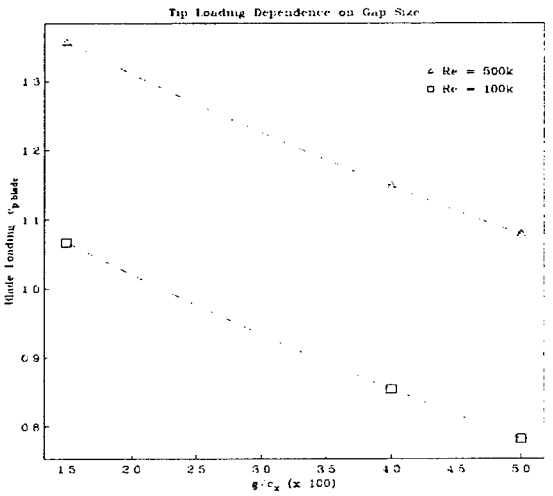

Figure 19 Blade loading as a function of g/c ratio.

Contour plots of the end-wall static pressure are shown in Figure 20. One interesting feature of the endwall contour plots is an isolated region of negative static pressures occurring directly over the blade. It is hypothesized that such a region of isolated static pressure indicates a high streamwise velocity departure of the tip leakage vortex from the blade tip. The point of departure moves forward with an increase in gap size and the departure region grows dramatically in all cases with Reynolds number. Interestingly, at the higher Reynolds number, the departure zone of the tip leakage flow becomes tighter as the gap increases. A direct correlation between the area of this departure zone over the blade tip and the overall blade loading is observed. Contour plots of g/c = 0.015 and g/c = 0.04 represent the cases with the greatest tip blade loading (Figure 19), and consequently contain the largest zone of the tip leakage flow departure. The greater the tip blade loading becomes, the larger the departure zone grows. The relationship is explained by a larger pressure gradient over the blade tip, which drives more mass flow into the gap and creates a larger tip vortex to depart from the pressure side edge and traverse the tip region. A strong streamwise velocity is also seen near the mean camber line in the departure zone and shortly upstream, indicating a dynamic streamwise motion tied to the tip leakage flow.

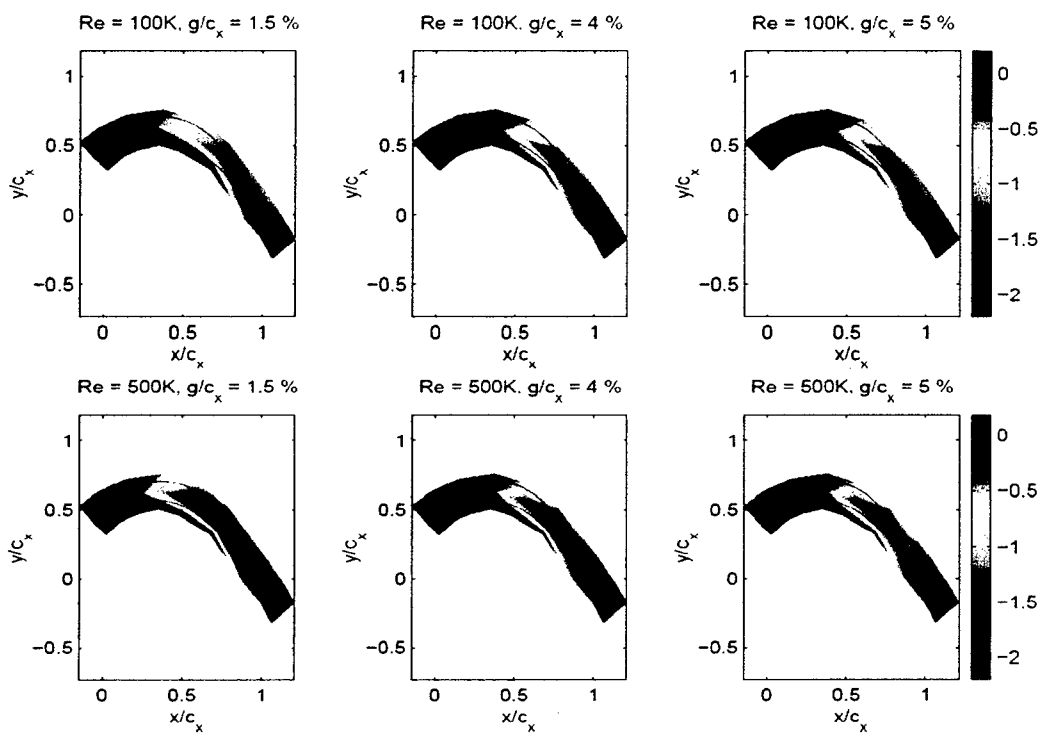

Figure 20 Tip endwall static pressure contours at various Reynolds number and g/c values.

Contour plots of nondimensional streamwise vorticity and total pressure loss confirm a significantly larger tip leakage vortex fed by enhanced gap discharge with larger gap. On the left side of the windows of Figure 21, a positive vorticity and the zero contour of λ_2 denotes the passage vortex contribution. A region of negative vorticity corresponds to the tip leakage vortex which enters into the top of the picture and is also outlined by the zero contour of the second eigenvalue of the velocity gradient tensor. Rapid changes in vorticity in this small, 1.5 in. by 2.0 in. window indicate a great deal of mixing and three-dimensionality. Because extremes of vorticity are consistently outlined by zero contours of λ_2, these contours are then superimposed on total pressure loss contours in Figure 21.

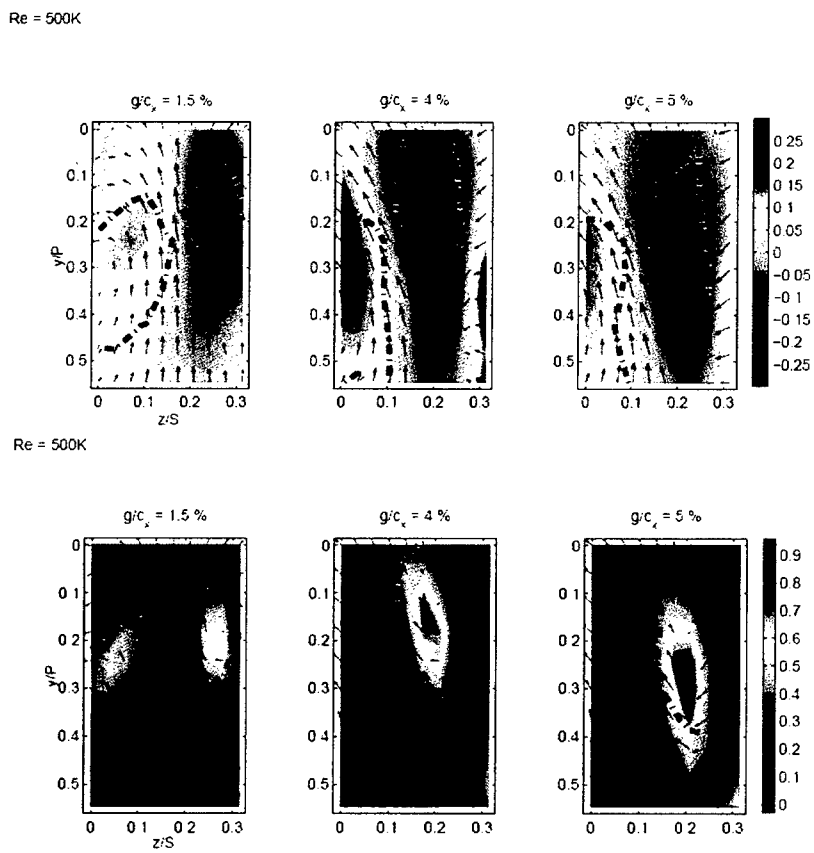

Figure 21 Flat tip vorticity and total pressure loss contours for various g/c ratios at Re=10^5.

The passage vortex is pushed to the left side of the window as the gap grows on the right side of the window. However, the passage vortex is also forced downward and the opposite vorticity associated with the tip vortex moves slightly lower and much closer to the endwall at larger gap

sizes. Secondary velocity vectors demonstrate a strong cross-passage fluid motion of the suction, low-pressure side between the two vortices. The tip vortex may be seen to move lower at each increase in the gap size. Lastly, strong secondary flow vectors are seen on the endwall at the two larger gap sizes while the fluid has very little secondary velocity component at the endwall in the 1.5% gap case. Undoubtedly the reason lies with the proximity of the tip leakage vortex to the endwall and the compactness of the vortex.

Although difficult to judge in the 4% gap case, the passage vortex certainly contains a higher region of loss at the largest gap setting than at 1.5%. Even though peaks in the loss can be seen in the passage vortex for these cases, attention should be called to the region between the two counter-rotating structures.

As the vortical structures move farther apart, the region of loss between them grows, which may discredit the idea that two close regions of vorticity generate greater loss due to the enhanced mixing. More loss is generated between the tip vortex and passage vortex in the two cases when they are farther apart than when they are in close proximity.

At the high Reynolds number, peaks in loss again are seen inside of vortices. The tip leakage vortex, mostly mixed out at Re = 1.0×10^5, now is clearly defined. The fringes of the passage and tip leakage vortex remain close to one another, but the centers of the two vortices appear to be closer in the g/c = 1.5% case. For this reason, the loss in the tip vortex does not peak as high and is instead shared with the passage vortex. At the lowest gap setting, the two vortices are clearly distinct and close together, and as a consequence the loss is concentrated inside the vortices themselves instead of distributed between them. As the vortices spread out in the wake, a region of low loss connects them and it is this region that must not be overlooked when considering the overall loss.

For each case, all of the peak loss regions are located in or near the core of a passage or tip vortex contour. Dominance of the tip leakage loss is obvious at the high Reynolds condition. Regions of loss associated with the tip and passage vortex are much more distinct as the vortices grow in strength as indicated by the vorticity magnitude and tightening of the vortex core. Plotting the overall mass-averaged total pressure loss against gap height gives Figure 22. Following increases in blade loading and gap discharge, overall total pressure loss substantially rises with Reynolds number. As the gap size grows, the total pressure loss in the wake increases in a nonlinear fashion.

If the gap height is increased by a factor of 3.3, a 68% rise in total pressure loss is observed for an upstream axial Reynolds number of 5.0×10^5. Over the same gap increase at a Reynolds number of 1.0×10^5, total pressure loss measured in the wake survey increases by 23%. An approximately equal change in total pressure loss coefficient is seen from one gap spacing to the next, which means that the effect is magnified at larger gap sizes. Obviously, sound design of turbine blades seeks to minimize the gap height and thus the discharge into the gap. However, the penalty in terms of total pressure loss increases disproportional at large tip clearances.

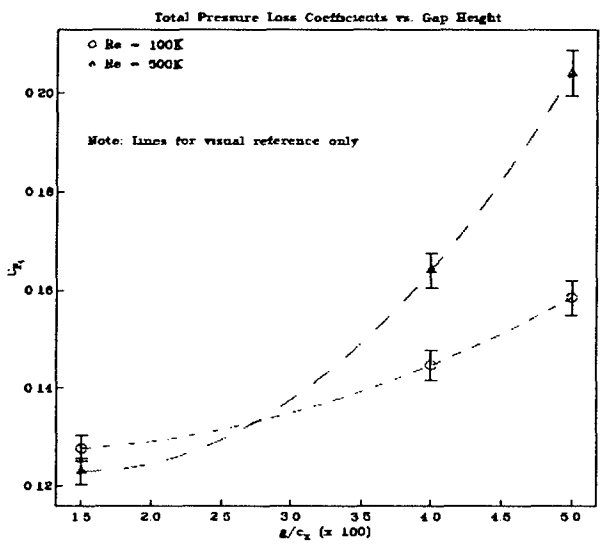

Figure 22 Mass averaged total pressure loss coefficients as a function of g/c at two Reynolds numbers.

5.3 Passive Flow Control by Squealer Tip

Documenting the squealer tip was first considered as a flow control strategy, where the gap size is judged in all cases to be the distance from the flat tip to the endwall, g. However, squealer tips are fabricated by milling out unnecessary blade tip material to leave a short ridge, which extends beyond the recessed flat tip surface. For this reason, the gap height is typically defined from the tip of the squealer to the tip endwall, deemed a true gap, τ, and portrayed in Figure 23.

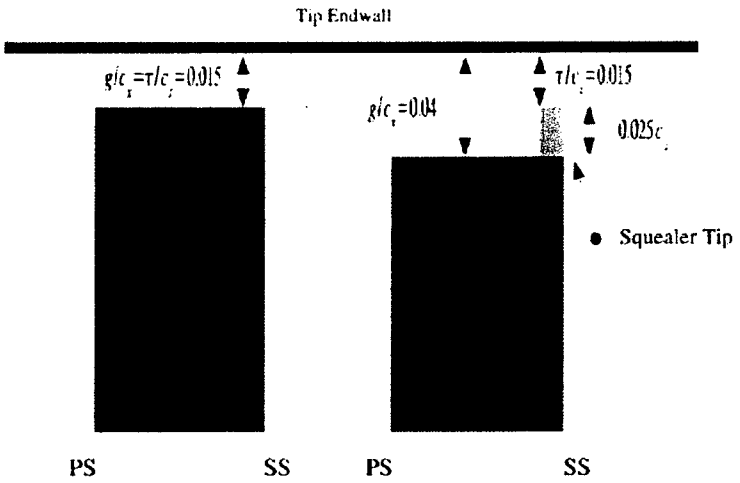

Figure 23 Geometry and definitions for flat and partial squealer cases.

Seeking to match some performance characteristics of the squealer tip with a future plasma actuator, the effect of the tip geometry modification was unconventionally documented at an equivalent effective gap, g/c. In addition to its aerodynamic performance, popularity of the squealer tip derives from its ability to limit gap discharge by extending the blade while posing less risk of a catastrophic blade rub than a full tip extension. The definition of the squealer tip as a blade extension is consistent with such a performance characteristic. Further, from the perspective of a flow control application, a flat tip was considered the "actuation off" case and a squealer tip was approached as the "actuation on" strategy. Consistent with these definitions, the squealer tip with a height of 0.025c was fixed to flat tip blades at g/c = 0.04 and g/c = 0.05.

Blade loading results are shown in Figure 24 for the flat and partial-squealer configurations. In a matter analogous to shrinking the gap, blade pressure distributions exhibit unloading at the leading edge and increased loading at the trailing edge of the suction surface. Addition of a squealer tip led to an increased blade loading in all cases. However, blade tip loading for the squealer configuration cases exhibits less drop as the gap is enlarged, hinting that the squealer tip blade loading is less sensitive to a change in gap size than the corresponding flat tip. A 1% change in gap size for the flat tip yields more than $0.05c_{p,blade}$ difference, greater than that seen for a similar

squealer tip gap change. This is especially true at the high speed squealer tip configuration where the blade loading appears to be the least sensitive to gap change.

The endwall pressure distributions are show for each test condition for the 4% gap cases in Figure 25. With a squealer tip configuration, the high velocity leakage jet shows that the departure from the tip gap is completely removed and a smooth acceleration through the passage is observed. Undoubtedly, the squealer tip reduces losses in the gap region due to a postponed and less violent separation from the blade tip, as proposed in the literature. For 4% gap size, the Reynolds number parameter, which shows heavy influence at the endwall for the flat tip, is largely ineffective in altering the endwall pressure profiles for the squealer tip. Even as the blade becomes much more loaded over the squealer tip, an observation which correlates with an increase in the departure activity for the flat tip, there is a lack of any noticeable difference for the squealer configuration. Existence of an enhanced pressure gradient but absence of the departure region means that the squealer tip stands as a fence to over-the-tip flow, through the entire blade chord. It is quite possible then that the tip leakage flow remains isolated over the blade throughout the entire tip gap and its losses are not fully appreciated until far downstream. With a squealer modification, endwall static pressure behavior becomes independent of Reynolds number as well as gap height.

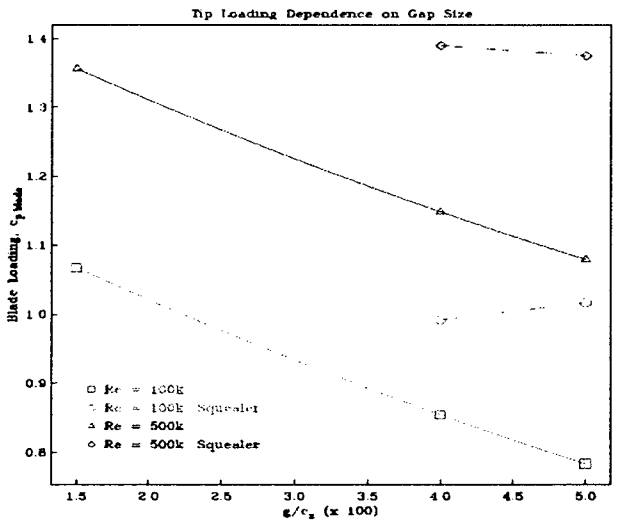

Figure 24 Blade loading as a function of g/c ratio comparison between flat and squealer tip configurations.

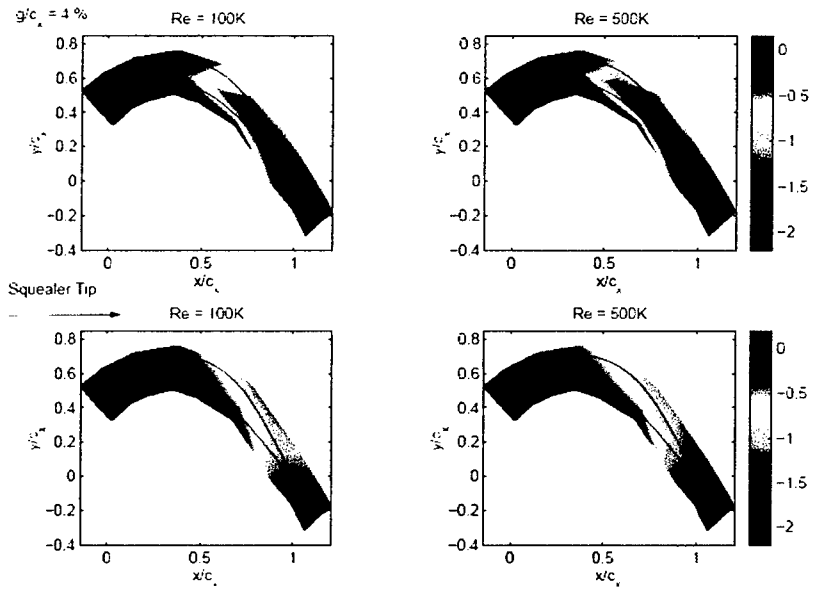

Figure 25 Comparison between endwall static pressure distributions for flat tips (top) and squealer tips (bottom).

Wake measurements for flat and squealer tips are shown in Figure 26. Tip leakage and passage vortices start far apart in Figure 26, move closest together at Re = $3.0\text{x}10^5$, and then move apart again at higher Reynolds numbers, similar to the trend in the flat tip case. Immediately noticed at low speeds is a much more coherent tip leakage vortex, possibly because it has travelled farther over the blade tip. Thus, the squealer tip leakage vortex has experienced less mixing than leakage flow over a flat tip, which departs the tip gap near 70% axial chord and undergoes intensified mixing through the remainder of the passage.

The tip leakage vortex is more distinct and smaller in size with the squealer configuration for $2.0\text{x}10^5 < \text{Re} < 5.0\text{x}10^5$, which can be explained by less mass flow into the tip gap feeding the tip leakage vortex and also a stalled departure from the tip gap and thus a less mixed leakage flow. Even at a full chord downstream, a tighter, less-mixed vortex is observed, and similar loss measurements taken upstream would likely show more improved squealer tip performance. An inverse relationship between tip and passage vortices in terms of vortex size denoted by λ_2 contours as well as the peak loss is observed for the squealer tip in Figure 26. At a slightly larger gap, similar results are expected and observed. While peak losses in the tip leakage vortex core are never reduced from those of a flat tip, reduction in total pressure loss from the squealer tip is

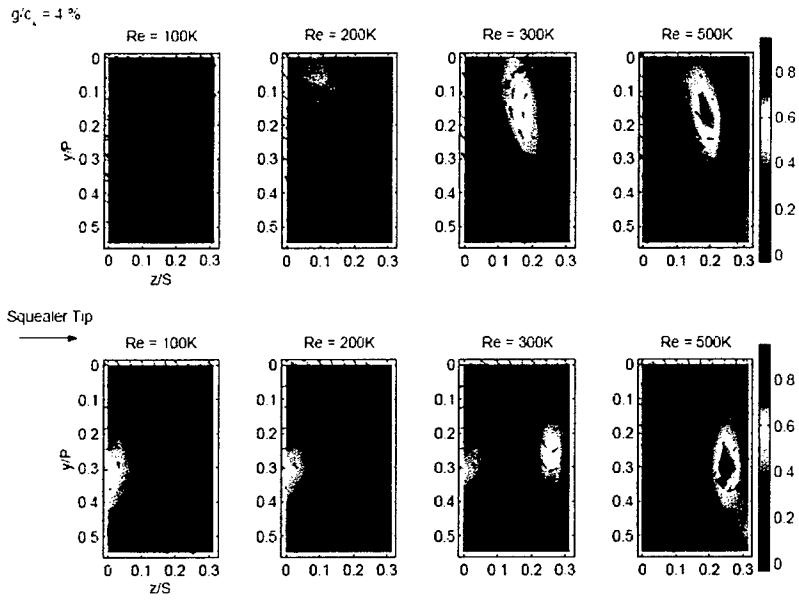

Figure 26 Comparison of total pressure loss distributions in blade wakes with flat tips (top) and squealer tips (bottom) for a range of Reynolds numbers.

attributed to a reduction in mixing of the tip leakage and passage vortices in respect to each other and the freestream.

Results of the loss studies are effectively summarized with Figure 27. For all cases, increasing the gap size increases the loss nonlinearly. For both Reynolds numbers, the squealer is effective at the 4% gap but largely ineffective at 5%. At 4% gap, even though peaks in the loss for the squealer tip exceed those for the flat tip, the absence of the extensive low loss regions of the flat tip case bring about a lower overall loss for the squealer configuration. At 5%, the structures are less distinct

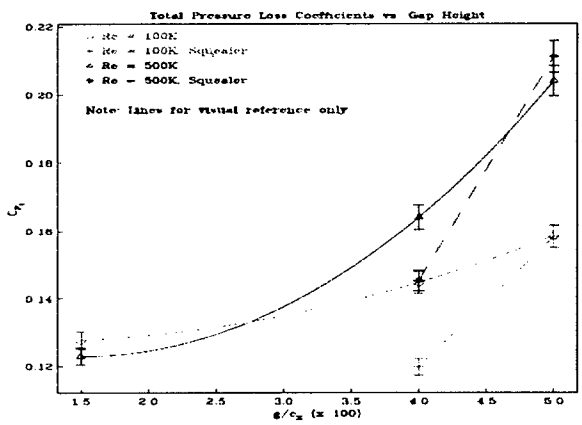

Figure 27 Effect of g/c ratio on mass-averaged total pressure loss coefficients for blades with flat tips and squealer tips.

and mixing between the major vortex actors creates large, undesirable low-loss regions, which eventually ruin the case for the squealer at 5%.

Noting a consistent change in squealer tip performance at both Reynolds numbers in the transition from g/c = 4% to g/c = 5%, a change in the flow field was suspected and the criteria defining a "thick" or "thin" blade, $\tau/g = 4.0$, was revisited. The distinction proposed by Denton (1993) for a flat tip is applied to the squealer tip configuration in Figure 28. In the case of a thick blade, flow separates on the pressure side edge, forms a separation bubble and reattaches, and then is restricted from flowing across the blade tip by the presence of a squealer tip. Fluid recirculates directly above the blade tip and effectively extends the blade. Flow forms a vena contracta above this squealer tip to further constrict the mass flow over the suction side.

A thin blade also features a complete separation of the flow from the pressure side corner. This time however, the presence of the squealer tip is not felt by tip gap flow and any available improvement is largely reduced. The distinction between thick and thin blades in this manner is found at a boundary of $\tau/g = 3.5$, which is near the approximate value of 4.0 proposed by Denton (1993).

5.4 Active Flow Control

The plasma squealer design was constructed in implemented in the high speed cascade setup for a direct comparison to the passive control results. When the blade was fitted with the actuator but no voltage was applied, the downstream wake was found to be different than the wake profiles obtained with the basic flat tip geometry previously studied. Figure 29 demonstrates this result at a Reynolds number of 5.0×10^5 and g/c = 4%. Sharp edge effects on similar blades have been doc-

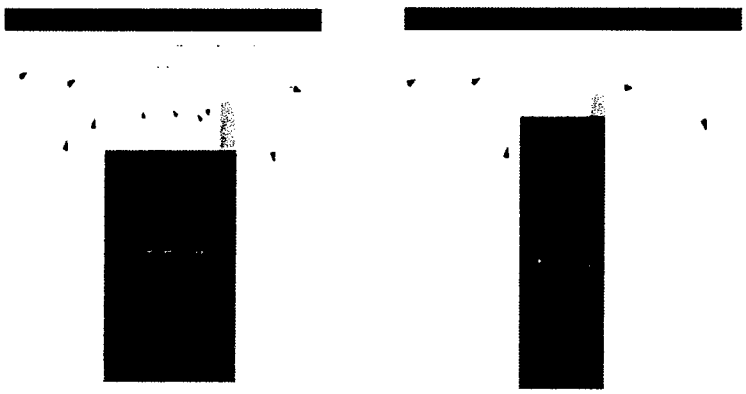

Figure 28 Flow models for the squealer tip corresponding to "thick" and "thin" blade scenarios.

umented by Bindon (1992), and Ameri (1999). The actuator has a sharper edge than the unmodified blade, and thus the baseline results are different than those obtained for the squealer. Thus, results cannot be directly compared. This also indicates that the flow is very sensitive to minute changes, and thus is a good candidate for applying active flow control.

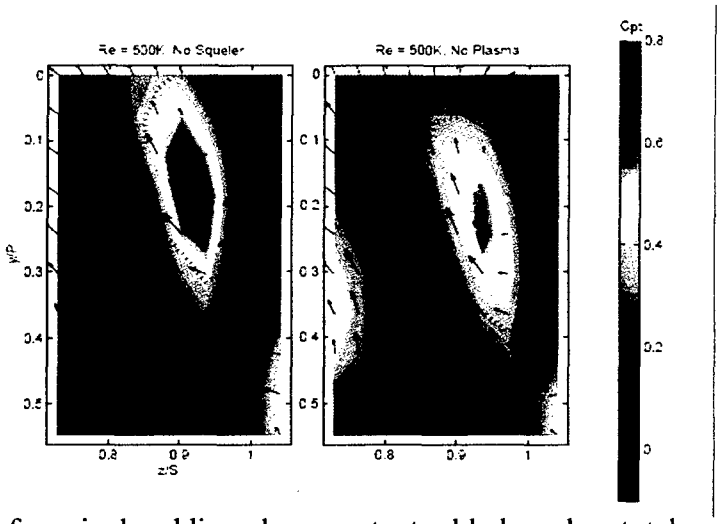

Figure 29 Effect of passively adding plasma actuator blade end on total pressure loss for basic flow at Re=5x10^5 and g/c=0.04.

Rather than attempting produce a steady blockage in the gap like the squealer tip, the plasma actuators were operated with an unsteady frequency that was meant to couple with instabilities inherent to the tip-gap flow. A sensitive location in the flow was identified, and a range of actuator frequencies were run to determine which had the strongest effect on the flow at a specified point in space. Figure 30 shows two spacial locations that were considered, with one being considered twice. Reynolds number was held constant at 5.0x10^5 and g/c was held at 0.04. The unsteady frequency of the plasma was varied between 100 Hz and 2100 Hz. For comparisons at different speeds the frequency was non-dimensionalized as

$$\beta = \frac{f * g}{U_2}. \tag{9}$$

where f is the frequency and U_2 is the upstream velocity. The two circled points in Figure 30 indicate the non-dimensional frequencies where the strongest effect on the flow at that point was

apparent. These are $\beta = 0.03$ corresponding to a frequency of 500 Hz at one location, and $\beta = 0.07$ corresponding to 1250 Hz at the other considered location.

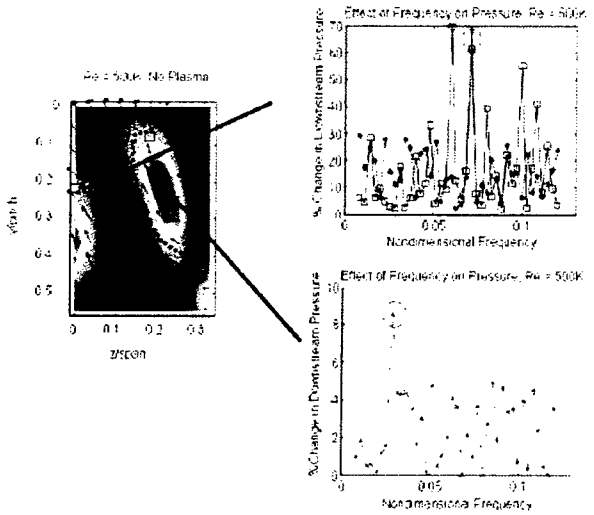

Figure 30 Effect of varying frequency on downstream total pressure measurements at specified locations in space based on sensitive areas shown in wake surveys.

These two non-dimensional frequencies were considered with the baseline case obtained with the actuator on the blade. Total pressure loss measurements in the wake of each of the three cases are shown in Figure 31. These show well defined leakage and passage vortices at Re = 5.0×10^5 and g/c = 0.04. The leakage vortex stays well defined, but weakened and shrank when the plasma actuator was operating. The higher frequency had a stronger affect. These results also indicate increased mixing of the vortices in the $\beta = 0.03$ case, eliminating the benefit of reducing the size and strength of the leakage vortex.

The endwall pressure distributions obtained using unsteady plasma at Reynolds numbers of 5.0×10^5 and g/c=0.04 are shown in Figure 32. Recall that when the squealer was applied, the region of high loss in the gap was no longer seen, as demonstrated in Figure 31. Now, however, the high leakage jet appears unaffected as the isolated region of negative static pressures is almost identical in all three plots. This could be due to the fact that the plasma does not fully block the flow. As a result, it is still allowed to pass through the gap as it otherwise would with the flat blade tip. This means that the high temperature air is not trapped in the gap when the plasma is used, as it is with the squealer tip, and that using the active flow control may reduce the risk of damage to the blade due to trapping hot air.

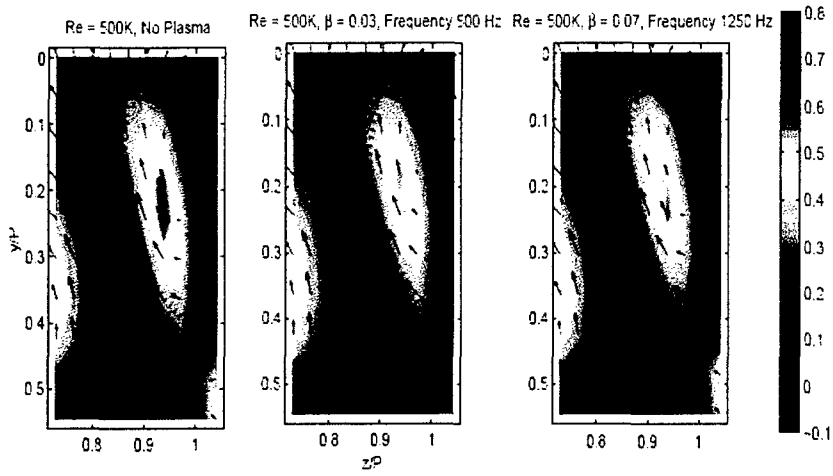

Figure 31 Effect of unsteady plasma forcing on total pressure loss distributions.

Mass averaged coefficients of pressure are shown in Figure 33. The pressure coefficients over the surveyed region showed negligible change between no actuation and actuation at $\beta = 0.03$. However, a significant change was seen for $\beta = 0.07$. It is not as significant as the difference between no squealer and squealer on, but it is an encouraging starting point for future research using active flow control with plasma actuators on turbomachinery.

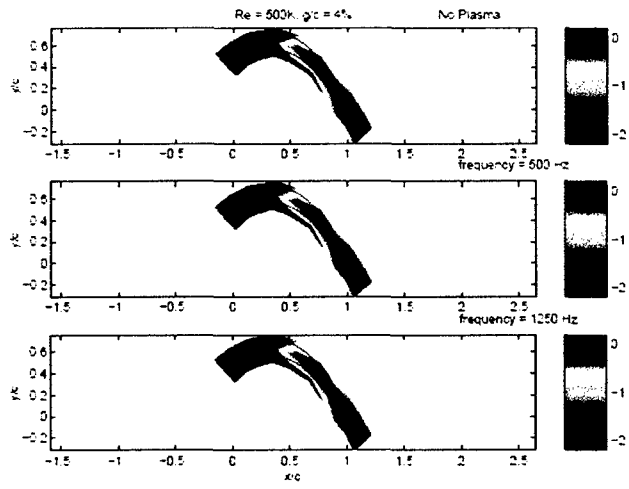

Figure 32 Tip endwall static pressure contours at different unsteady plasma frequencies.

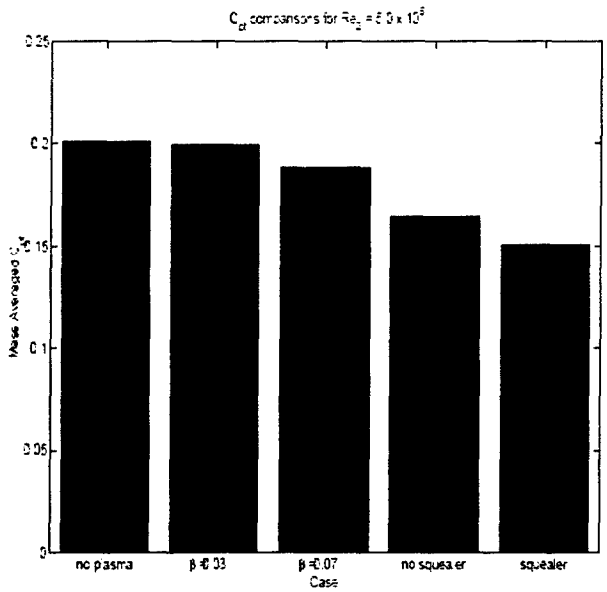

Figure 33 Mass averaged coefficients of pressure for the surveyed region at five considered actuation cases at Re=5.0x10^5 and g/c=0.04.

5.5 Conclusions

Although complications of the tip leakage and passage vortices do not pose an entirely new problem, data sets in the literature to date have failed to fully explore and compare the effects of Reynolds number and gap size for flat and suction-side squealer tip geometries. Further, most cascade work to date has dealt with low Reynolds numbers, which is shown to be a limiting condition. Flat tip results serve as the baseline condition. In terms of blade loading, an increase in gap size results in unloading over the entire pressure surface and at the leading edge of the suction surface, and enhanced loading on the suction side at the trailing edge. Increasing Reynolds number increases blade loading along the entire suction surface. A tip leakage vortex departure zone is centered 60-80% of chord, is independent of gap size, and undergoes substantial growth with Reynolds number. Peak losses in the wake are associated with tip leakage and passage vortices. Larger gap sizes permit greater gap discharge which increases passage and tip leakage vortex size, peak loss, and mixing loss. Reynolds number is critical in strengthening and reordering wake vortical structures and feeds loss mechanisms.

In a manner analogous to shrinking the gap, the squealer tip reduces gap discharge and increases blade loading. Once the squealer tip has been added, endwall pressure distributions indicate a complete elimination of the departure zone, leaving only a smooth acceleration through the pas-

sage. It is hypothesized that the squealer tip stands as a fence to the leakage jet and permits the vortex to either slowly trickle over the suction edge or to remain over the tip surface until the trailing edge.

Qualitatively, adding a squealer tip yields changes similar to those seen when reducing gap size. Structures become more clearly defined with strong vorticity and local loss regions and their interaction is reduced. With a squealer tip, the loss is derived predominantly inside the two vortices and expansive regions of low mixing loss are largely reduced. An inverse relationship between the tip leakage and passage vortex loss and overall size is observed as Reynolds number is increased. The squealer tip is notably more effective at $g/c = 0.04$ and fails to yield any improvement at $g/c = 0.05$, where a peak in tip leakage loss overrides gains from the organization of the wake. It is hypothesized that a different flow model corresponds to this larger gap scenario, where leakage flow separates from the pressure side edge and bypasses the squealer tip entirely. Revisiting Denton's (1993) criteria to divide a thick and thin blade flow condition, a reduced value of $\tau/g = 3.5$ was found to match results for this data set.

Adding an actuator to the end of the blade modifies the geometry enough to affect the baseline flow, indicating a very strong sensitivity to changes making this set-up a good candidate for flow control observations. Running the plasma at unsteady frequencies excites natural instabilities and finding an optimum frequency should have a strong effect on the flow. When run at an unsteady non-dimensional frequency of $\beta = 0.03$ or $\beta = 0.07$ the actuator is seen to cause the leakage vortex to shrink in both size and strength. However, the jet leakage seen on endwall pressure readings is unchanged, indicating that the flow is not being trapped in the gap. Future research will include larger surveys on the wake region and consideration of higher unsteady frequencies.

6.0 EFFECTS OF BLADE THICKNESS ON PASSIVE AND ACTIVE CONTROL RESULTS

The experimental results presented in this section are focused on the independent effects of thickness-to-gap and gap-to-chord ratios on the tip-gap flow behavior. Two extreme gap-to-chord ratios of 5% and 8% were chosen, for which four thickness-to-gap ratios were examined. The flow was documented through blade-tip and end-wall static pressure measurements, and downstream total pressure loss coefficients. Additionally, surface flow visualization was performed on the blade tip end for a greater understanding of the gap-flow behavior.

The response of the flow to passive flow control using a partial suction-side squealer tip at each of the thickness-to-gap and gap-to-chord cases was documented. The intention was to examine any sensitivity of the flow to the gap-to-chord ratio that might be attributed to the thickness-to-gap ratio in a manner that can be categorized as "thick" and "thin" blade behavior. For this the focus was on possible changes in the size and location of a separation and re-attachment lines on the blade tip end. Defining such features in these flows is important to our goal of active tip-gap flow control using plasma actuators because they are highly receptive to unsteady forcing.

The previous section described results of passive flow control using a partial suction-side squealer in which the tip flow became less sensitive to a squealer tip when the blade thickness-to-gap ratio was less than 4. Denton (1993) proposed that the behavior of the flow in the gap changes with the thickness-to-gap ratio. He found that if the blade thickness is more than about four times the gap size, the flow behaves as a "thick" blade. The flow topology of a "thick" blade consisted of a a separation and re-attachment line that formed on the blade tip.

If the blade were "thin" according to Denton (1993), the flow separates from the pressure-side blade edge and never re-attaches on the blase tip. Figure 34 depicts the flow topology of "thick" and "thin" blades. The results shown in Section 5 indicated a slightly different threshold between "thick-thin" behavior that was at a $\tau/c=3.5$.

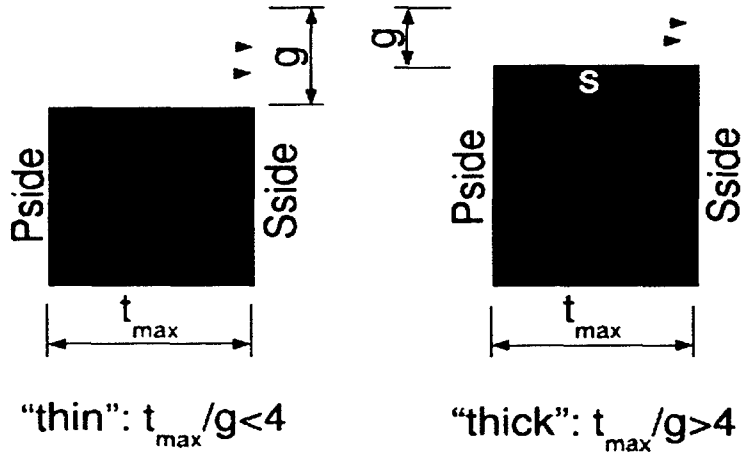

Figure 34 Schematic of flow topology that distinguishes between "thick" and "thin" blades.

The objective of the experiments presented in this section was to study the independent effects of thickness-to-gap and gap-to-chord ratios on the flow topology associated with "thick" and "thin" blades. This involved two extreme gap-to-chord ratios of 5% and 8%, and four thickness-to-gap ratios. The differences in the flow resulting from these conditions were documented by blade-tip and end-wall static pressure measurements, as well as downstream total pressure loss coefficients. Additionally, flow visualization was performed on the blade tip end to document flow separation and re-attachment characteristics. The response of the flow to passive flow control using a partial suction side squealer at each of the thickness-to-gap and gap-to-chord cases was then documented. The sensitivity of the flow to combinations of thickness-to-gap and gap-to-chord ratios with respect to the published "thick" and "thin" blade categories was then summarized. These results are then put in context with a change in the size and location of a separation and re-attachment line on the blade tip end. Defining the location of separation and re-attachment lines is important to our goal of active tip-gap flow control using plasma actuators because such flow features are traditionally highly receptive to unsteady forcing. The ultimate intention is to affect the tip-vortex formation and downstream mixing by exciting an instability of the blade-gap flow by unsteady forcing through a plasma actuator located on the blade tip.

6.1 Experimental Setup

The present experiments were obtained in the high speed cascade described in Section 2. All of the cases in this study were performed at an inlet Reynolds number of 0.5×10^6, corresponding to

an inlet Mach number of 0.2 and an exit Mach number of 0.3. Removable plastic shim spacers shaped like the blade profile were added to the center blade to provide different gap spacings. The shims permitted gap sizes of up to 0.08c.

All three of the blades in the cascade were cast in a two-part epoxy from a numerically machined mold. The center blade was divided into three parts: a main molded blade with a span of 3.42 in., a removable molded blade segment with a span of 0.1875 in., and removable blade tip winglets made of glass epoxy board with a thickness of 0.0625 in. One end of the main blade segment was attached to the back wall of the cascade section. The 0.1875 in. removable segment was attached to the other end of the main blade segment. Spacers with the same blade profile could be placed between the removable blade segment and the main blade to vary the distance between the blade end and the front wall of the cascade section.

The winglets were machined using a numerically controlled milling machine from 0.0625 in. thick glass-epoxy boards that were originally copper-clad on both sides. The copper cladding was also machined off using the same milling machine to leave electrodes that were a part of the plasma actuator when active control was done.

A set of different size winglets were produced. A photograph of these are shown in Figure 35. The winglets used with the 5% gap-to-chord are shown as the left column in the photograph. Those used with the 8% gap-to-chord are shown as the right column. For the 5% gap-to-chord ratio, these gave thickness-to-gap ratios of 2.83, 3.3, 3.7, and 4.3. For the 8% gap-to-chord ratio, these gave thickness-to-gap ratios of 1.75, 2.83, 3.3, and 3.7.

The squealer used in the experiments was a partial, suction-side type. It consisted of a 0.031 in. thick metal strip that was contoured to the shape of the blade profile and bonded to its end. The height of the strip was τ=0.1035in. which corresponded to τ/c=0.025. It did not change in height with changes in the thickness-to-gap. The partial squealer extended over the center 75% of the blade profile. It can be seen mounted on the end of a blade in the photograph in Figure 35.

Static pressure taps were located at the end of the main blade portion of the center blade. These provided measurement of the static pressure near the end of the blade. Because they were on the edge of the main blade, their location relative to the end of the built-up blade changed as spacers were added to vary the tip-gap. As an example, for the 8% gap-to-chord case, the pressure taps were 0.06c from the tip, while for the 5% gap-to-chord case, the pressure taps were 0.09c from the

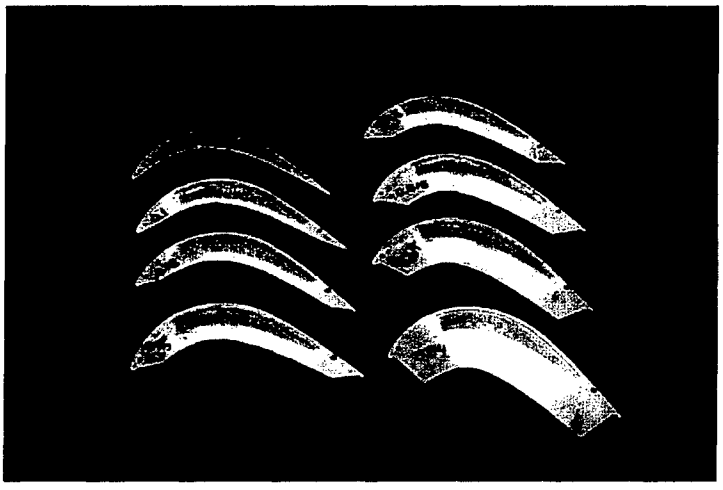

Figure 35 Photograph of winglets used to create various thickness-to-gap ratios on the measurement Pak-B blade. The left set was used with the 5% gap-to-chord setup. The right set was used with the 8% gap-to-chord setup.

tip. Thirty (30) static pressure ports were also located on the end-wall under the blade. The flow field in the wake of the center blade was documented using a five-hole Pitot probe as described in previous sections of this report.

The method of surface flow visualization followed that of Langston (1982) and Aunapu (2000). This involved covering the tip of the blade with a white contact paper. An extra-fine point water-proof marker was used to make black dots in a pattern on the paper. An air brush was then used to spray on a thin wet coating of methyl salicylate (also known as oil of winter green) on the paper. The methyl salicylate absorbed the marker ink so that when the tunnel was turned on and brought quickly up to speed, the ink was transported by the local surface shear stress. When the tunnel was turned off and the methyl salicylate completely evaporated, the ink traces were fixed to the contact paper. The paper was then removed and digitally scanned. Three surface flow visualization runs were performed for each experimental condition. The images from the runs were then averaged.

6.2 Results

Contour plots of the total pressure loss in the wake along with the corresponding velocity vectors for all the thickness-to-gaps at g/c=0.05 are shown in Figure 36. The flat tip cases are shown as the top row, and the squealer tip cases are shown as the bottom row. Note that the wall is at the right edge of each plot, and the blade-end/wall intersection is at the upper right corner of each plot.

The highest loss coefficients (yellow with red region) are associated with the tip-gap vortex. Both a change in the magnitude and center location of the maximum loss coefficient are observed to occur by changing t/g, with and without the squealer tip. In order to try to quantify the motion of the center of the maximum loss coefficient, its y-z position was defined as

$|yz|^2 = (y/pitch)^2 + (z/pitch)^2$. This is presented as a function of the t/g for the 5% g/c in Figure 37.

For the baseline flat tip case, the location of the maximum loss coefficient center changes almost linearly with t/g up to t/g=3.5. This is close to the t/g criteria for "thick" blades given in Section 5. Beyond that t/g, the location of the maximum loss coefficient center is insensitive to the thickness-to-gap ratio.With the addition of the squealer, the maximum loss coefficient location is closer to the end wall, and its position is less sensitive to the change in the thickness-to-gap ratio.

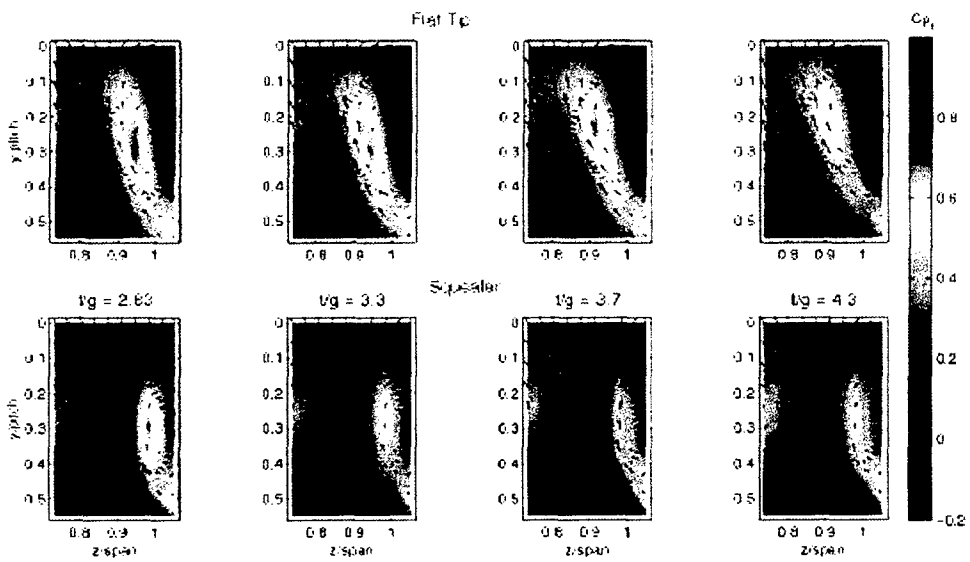

Figure 36 Coefficient of pressure distribution for different winglets producing different thickness-to-gap ratios for a 5% gap to chord ratio.

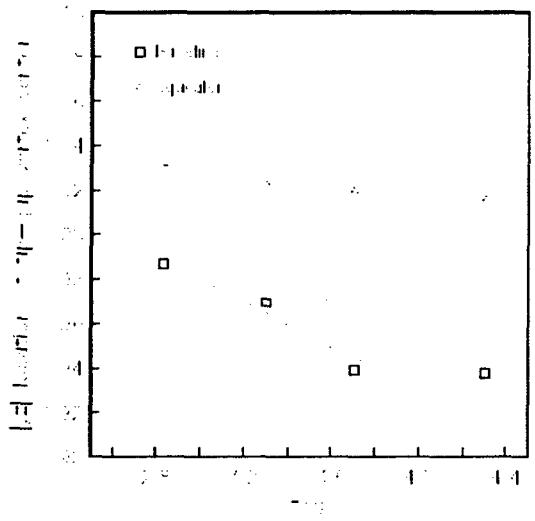

Figure 37 Magnitudes of the locations of the center of the tip-gap vortex as a function of the thickness-to-gap ratio at a 5% gap-to-chord ratio

Contour plots of the total pressure loss in the wake along with the corresponding velocity vectors for all the thickness-to-gaps at a 8% g/c are shown in Figure 38. The flat tip cases are shown as the top row, and the squealer tip cases are shown as the bottom row. Again the highest loss coefficients (red regions) are associated with the tip-gap vortex. The magnitude and center location of the maximum loss coefficient are again observed to depend on the t/g, and the addition of the squealer tip. The position of the maximum loss coefficient center is presented as a function of the t/g for g/c=0.08 in Figure 39.

For the baseline flat tip case, the location of the maximum loss coefficient center again changed almost linearly with the thickness-to-gap ratio up to t/g=3.5. For t/g>3.5, its location was asymptoting in a manner similar to the g/c=0.05 case.

With the addition of the squealer, the tip-gap vortex location was closer to the end wall, and its position became less sensitive to the change in the thickness-to-gap ratio at a slightly lower t/g=3.0.

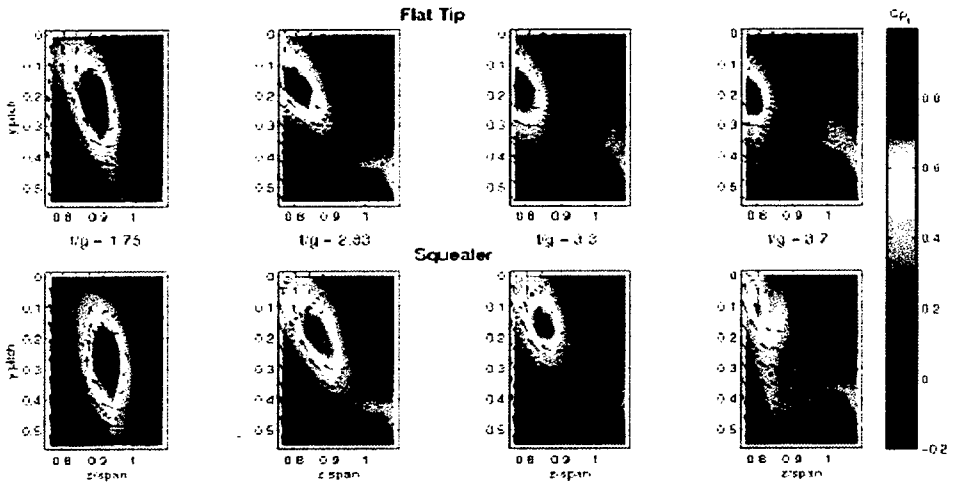

Figure 38 Coefficient of pressure distribution for different winglets producing different thickness-to-gap ratios for a 8% gap to chord ratio.

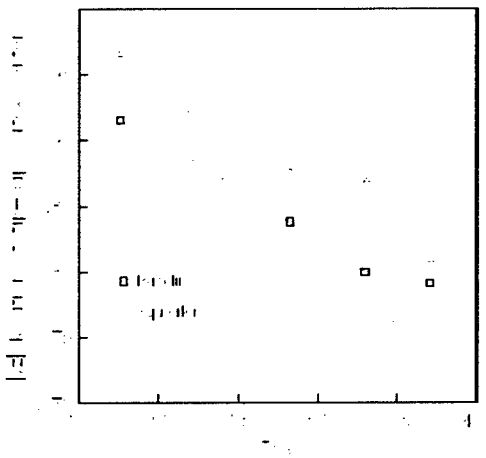

Figure 39 Magnitudes of the locations of the center of the tip-gap vortex as a function of the thickness-to-gap ratio at a 8% gap-to-chord ratio.

Pressure distributions at the end of the blade near the tip for the g/c=0.05 at all of the thickness-to-gap values are plotted in Figure 40. The solid line connecting points corresponds to the pressure distribution at the mid-span of the blade with the tip-gap closed. The dotted curve corresponds to the distribution from an Euler simulation for infinite aspect ratio Pak-B blades. Both of these are shown for reference.

The pressure distributions for the different t/g ratios roughly overlay each other except at the trailing edge on the suction side of the blade. The larger negative C_p values near the trailing edge are

indicative of the tip-gap vortex. This appears to be stronger for the smaller thickness-to-gap values. In addition the change with t/g ratio seems to decrease for t/g > 3.7, which is the approximate transition from "thin" to "thick" blades.

Integrating the C_p distributions in Figure 40 provides a measure of the blade loading near the tip. The blade loading for the g/c=0.05 is shown in Figure 41. For the baseline flat-tip case, the blade loading initially decreases with increasing t/g up to t/g=3.5. For t/g>3.5, the blade loading increases slightly then asymptotes.

The addition of the squealer tip increases the tip loading for all of the thickness-to-gap ratios at the g/c=0.05. The trend with g/c generally follows that of the baseline case, with a minimum blade loading occurring at the same t/g=3.5.

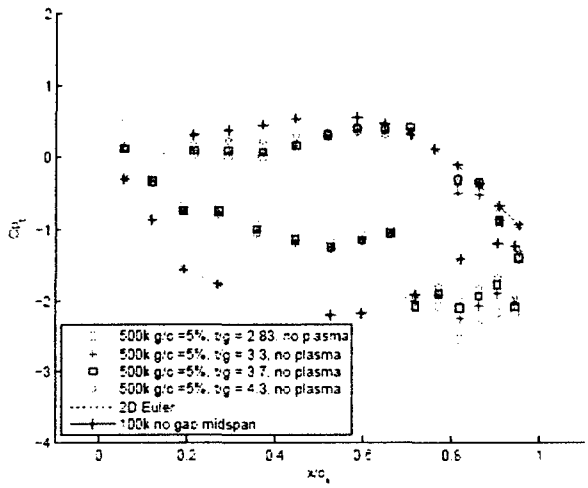

Figure 40 Pressure coefficient distribution at the end of the blade near the tip for a 5% gap-to-chord ratio and a range of thickness-to-gap ratios. Note no squealer installed.

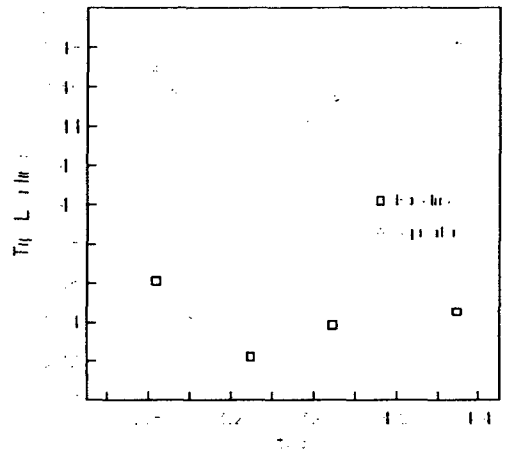

Figure 41 Blade loading as a function of thickness-to-gap ratio for a gap-to-chord ratio of 5%, with and without a squealer tip installed

Pressure distributions at the end of the blade near the tip for the g/c=0.08 at all of the thickness-to-gap values are plotted in Figure 42. Again for reference, the solid line connecting points corresponds to the pressure distribution at the mid-span of the blade with the tip-gap closed, and the dotted curve corresponds to the distribution from an Euler simulation for infinite aspect ratio Pak-B blades.

Again the pressure distributions for the different t/g ratios are observed to roughly overlay each other except at the trailing edge on the suction side of the blade. The larger negative C_p values near the trailing edge indicate a stronger tip-gap vortex than with the smaller g/c. Also in contrast to the smaller gap-to-chord case, the strength of the vortex appears to continually increase with increasing t/g.

Integrating C_p distributions in Figure 42 provides a measure of the blade loading near the tip. This is shown in Figure 43. The effect of t/g on the blade loading for the g/c=0.08 is quite different from the g/c=0.05 case. Although there is a good deal of scatter in the results for the baseline flat-tip case, the general trend is an almost linear increase in the blade loading with increasing t/g. This apparently is a result of an increase in the strength of the tip-gap vortex as t/g increases. Note that most of the t/g values are within the "thin" blade regime.

The addition of the squealer tip increases the blade loading at the lowest t/g, but subsequently decreases the blade loading at all the other larger t/g values. This points out the complexity of how the blade loading depends on a combination of the tip-gap blockage and the tip vortex strength.

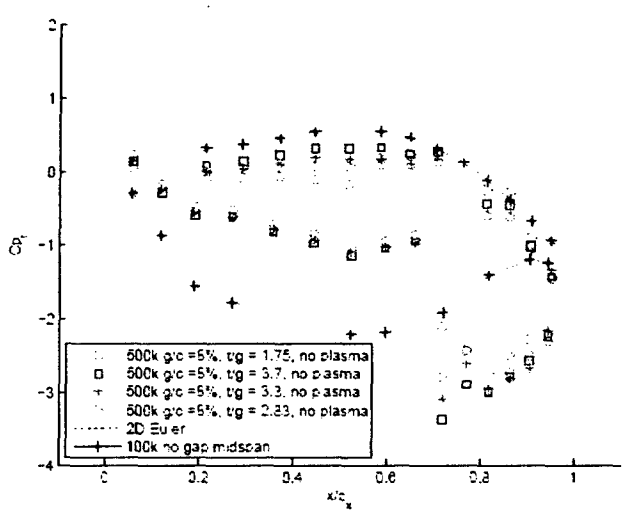

Figure 42 Pressure coefficient distribution at the end of the blade near the tip for a 8% gap-to-chord ratio and a range of thickness-to-gap ratios. Note no squealer installed.

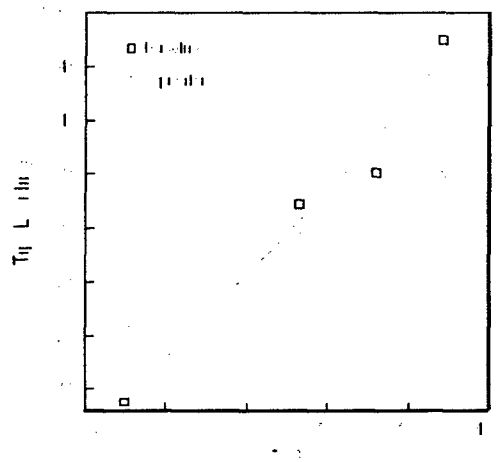

Figure 43 Blade loading as a function of thickness-to-gap ratio for a gap-to-chord ratio of 8%, with and without a squealer tip installed.

More insight into the differences observed in the wake measurements and blade-tip loading was obtained from the surface flow visualization on the blade tips. These are shown for the g/c=0.05 in Figure 44, and for the g/c=0.08 case in Figure 45. Recall that these surface visualization records consist of the tracks of ink dots that are assumed to follow the local shear stress on the end of blade that results from the flow through the gap. Three independent records were taken for each case, scanned digitally and averaged. Arrows have been added to provide an interpretation of the dot tracks. Viewing the surface visualization records, there are a number of obvious features.

1. There is a well defined re-attachment line at which the shear direction bifurcates, with some vectors pointed towards the suction side, and others pointed towards the pressure side of the blade.
2. The arrows pointing towards the pressure side suggest a flow recirculation from the re-attachment point to the edge of the pressure side of the blade.
3. There is a well delineated portion of the blade at the leading edge at which the shear vectors indicate that the passage flow traverses through the gap without re-attaching on the blade.

Given these characteristic features of the surface visualization at the 5% and 8% g/c, the following can be concluded.

1. The region where the passage flow traverses through the gap without re-attaching on the blade moves further back along the chord of the blade as t/g increases.
2. The chordwise extent of the re-attachment line shortens as t/g increases.
3. The chordwise extent of the re-attachment line shortens as g/c increases, even for the same thickness-to-gap ratio.

These results contradict the Denton (1993) proposal that for "thin" blades the flow separates from pressure-side edge of the blade tip but never re-attaches. In fact, the opposite appears to be the case. To aid in illustrating this, the length of the region where the flow does not re-attach as a percentage of the blade chord is plotted in Figure 46. In both g/c cases, the extent where the flow does not re-attach increases linearly with t/g. This is opposite to the trend postulated by Denton (1993).

In addition with regards to the topology of the flow under the blade, there does not appear to be a sharp transition such as one would quantify as a "regime". Rather the change in topology appears to be relatively smoothly changing with t/g.

Aside from the designation of regimes, the existence and extent of the re-attachment line is important for active flow control because it represents a very receptive site for unsteady forcing. Since the re-attachment line was found to essentially extend to the trailing edge of the blade, its length corresponds to $1-(x/c)_{no-reattachment}$ in Figure 46. That length decreases as either t/g increases or g/c increases.

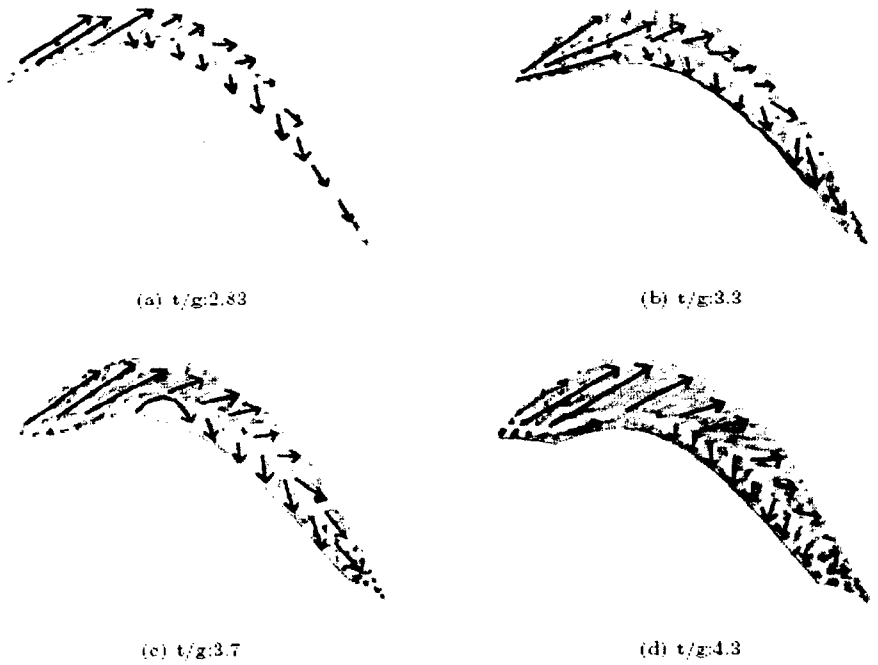

Figure 44 Surface flow visualization at the blade tip for a range of thickness-to-chord ratios at a gap-to-chord ratio of 5\%. Note no squealer installed.

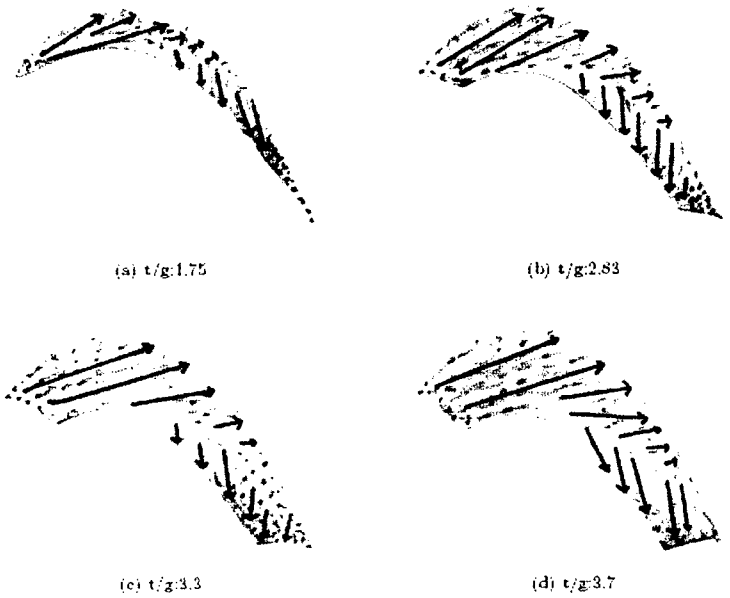

Figure 45 Surface flow visualization at the blade tip for a range of thickness-to-chord ratios at a gap-to-chord ratio of 8%. Note no squealer installed.

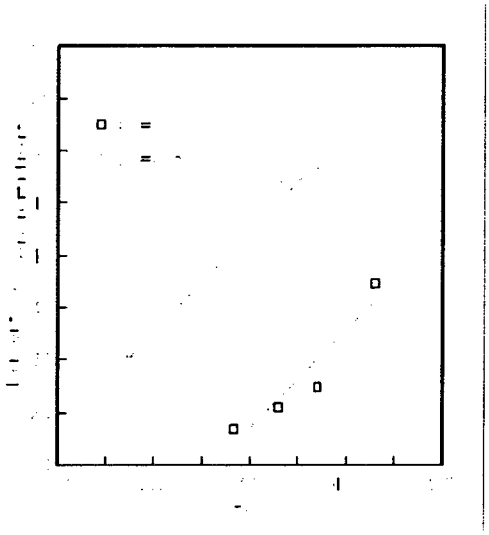

Figure 46 Length of region without re-attachment as a percentage of x-chord as a function of thickness-to-gap ratio for g/c=0.05 and 0.08.

The surface flow visualization was also examined for the cases with the squealer tip. These are shown for the g/c=0.05 in Figures 47 and 48, and for g/c=0.08 in Figures 49 and 50. Included with these are the surface flow visualization for the baseline cases that correspond to the squealer condition. Shown below the surface visualization are the corresponding wall pressure coefficient distributions. The color bar scales are the same for figures with the same g/c ratios. The location of the squealer is drawn on the surface visualization record as a thick black line.

The case with the g/c=0.05 for t/g=3.3 is shown in Figure 47. The condition would nominally be in the "thin" blade region. As previously shown from the surface flow visualization for the baseline flat-tip blade, a region near the leading edge is observed in which the flow passes under the blade without re-attaching. Also observed is the bifurcation line for the vectors that we associated with the re-attachment of the separation bubble from the pressure-side edge of the blade. The corresponding pressure field is consistent with this interpretation. The flow in the gap-passage near the leading-edge of the blade appears as the highest positive C_p value. The region of the re-attachment line on the blade end appears as the largest negative (suction) pressure coefficients on the

wall under the blade. The maximum suction pressure on the wall is at the trailing edge of the blade and probably reflects the effect of the tip-gap vortex.

The addition of the squealer tip has a dramatic effect on the flow under the blade as evidenced by the surface flow visualization and wall pressure distribution. The surface flow visualization indicates that a majority of the flow under the blade is turned, suggesting a large recirculation zone. The chordwise extent of this is comparable to the baseline case. The flow near the leading edge is turned by the squealer and vectored along the chord direction of the blade, feeding the recirculation zone. This large circulation formed by the squealer is a major drawback of this passive flow control because it would enhance heat transfer that could erode the blade tip.

With regards to the wall pressure distribution, higher C_p values occur on the pressure side of the blade with the squealer tip. The suction pressure at the trailing edge in this case appears lower, possibly indicating a weakening of the tip-gap vortex. Overall however, the blade tip loading was higher as was shown in Figure 43.

The case with the 5% gap-to-chord for t/g=4.3 is shown in Figure 48. This condition would nominally be in the "thick" blade regime. The corresponding pressure field is shown below the surface visualization. Overall the behavior is similar to the that at the smaller g/c value.

The addition of the squealer tip again has a similar dramatic effect on the flow under the blade. For the base flow, the larger t/g results in a larger portion of the flow at the leading edge that would normally pass through the gap without attaching to the underside of the blade tip. This flow is captured by the squealer tip and vectored along the chord direction of the blade. This resulted in higher shear on the blade surface that was evidenced in the longer ink streaks. These changes are visible in the wall pressure distribution especially near the trailing edge where the C_p values are noticeably higher (less negative) than in the flat-tip case. This is consistent with the measured increase in the blade tip loading (Figure 41).

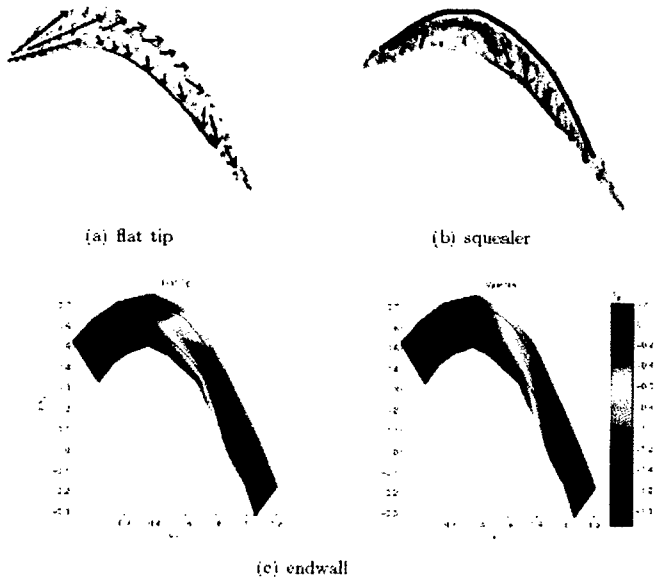

Figure 47 Surface flow visualization at the blade tip and pressure coefficient readings on the end-wall for a gap-to-chord ratio of 5% and a thickness-to-gap of 3.3 with and without squealer

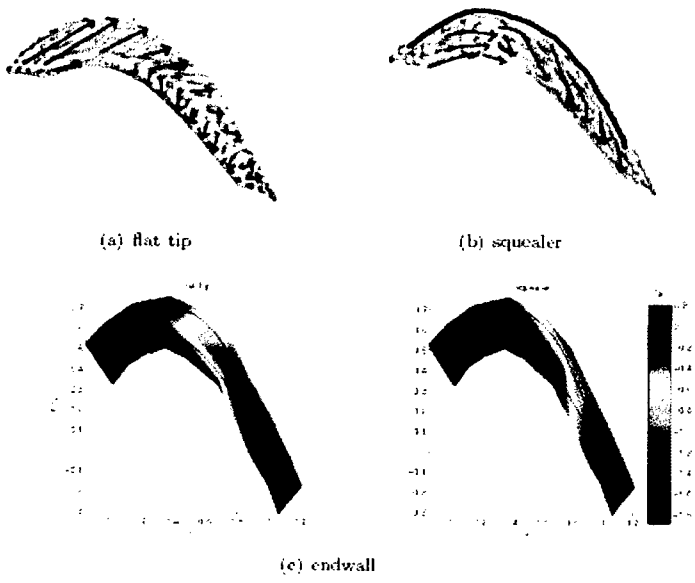

Figure 48 Surface flow visualization at the blade tip and pressure coefficient readings on the endwall for a gap-to-chord ratio of 5% and a thickness-to-gap of 4.3 with and without squealer.

Figures 49 and 50 document the effect of the squealer tip on the surface flow visualization and wall pressure for the g/c0.08. Figure 49 corresponds to t/g=2.83 which is nominally in the "thin" blade regime, and Figure 50 corresponds to t/g=3.7 which is on the lower edge of the "thick" blade regime.

The surface visualization for the g/c=0.08 baseline cases show the further lengthening of the region near the leading edge in which the flow passes under the blade without re-attaching. For the smaller t/g=2.83 case, the addition of the squealer tip redirects the flow near the tip as before. However one difference that is evident with the squealer tip on the larger g/c blade is a line of high shear that occurs close to and follows the edge of the pressure side of the downstream 60% of the blade. Whatever the significance of this, the wall pressure distribution indicated very little change with the addition of the squealer tip, and only a slight increase in the blade tip loading (Figure 43).

Although the larger t/g=3.7 at g/c=0.08, had shown more of a blade-tip loading increase with the squealer compared to the smaller t/g, there was not any significant change in the flow topology evident in the surface flow visualization or wall pressure distributions.

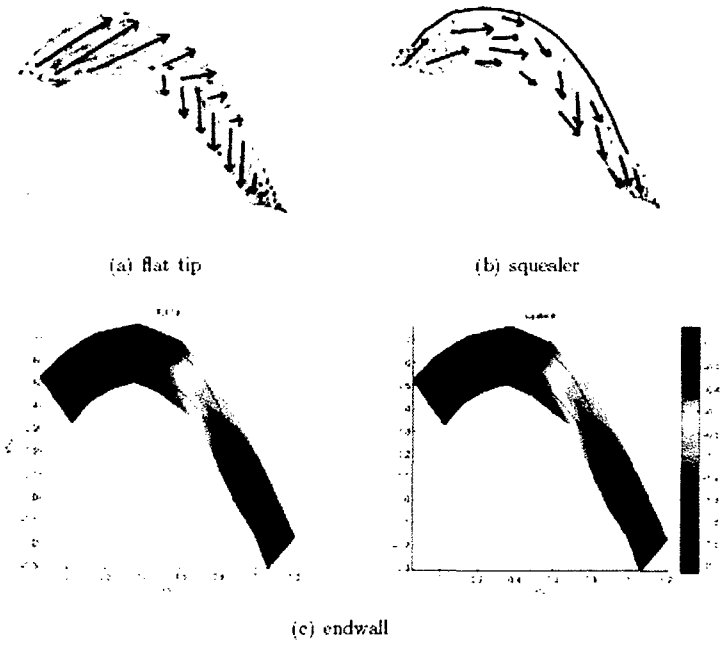

Figure 49 Surface flow visualization at the blade tip and pressure coefficient readings on the endwall for a gap-to-chord ratio of 8% and a thickness-to-gap of 2.83 with and without squealer.

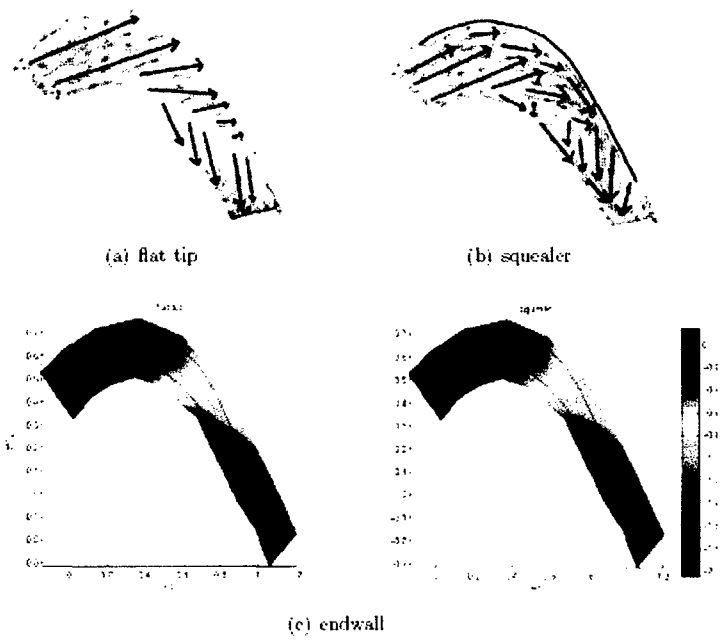

Figure 50 Surface flow visualization at the blade tip and pressure coefficient readings on the endwall for a gap-to-chord ratio of 8% and a thickness-to-gap of 3.7 with and without squealer.

6.3 Conclusions

An experiment was conducted in a linear cascade of Pak-B blades for an exit Mach number of 0.3 to simulate the flow in the tip gap region of a low pressure turbine blade row. The experiment focused on the independent effects of thickness-to-gap and gap-to-chord ratios on the flow behavior. Two extreme gap-to-chord ratios of 5% and 8% were chosen, for which four thickness-to-gap ratios were examined. The flow was documented through blade-tip and end-wall static pressure measurements, and downstream total pressure loss coefficients. Additionally, surface flow visualization was performed on the blade tip end for a greater understanding of the gap-flow behavior. The response of the flow to passive flow control using a partial suction-side squealer tip at each of the thickness-to-gap and gap-to-chord cases was documented. The intention was to examine any sensitivity of the flow to the gap-to-chord ratio that might be attributed to the thickness-to-gap ratio in a manner that can be categorized as "thick" and "thin" blade behavior. For this, the focus was on possible changes in the size and location of a separation and re-attachment line on the blade tip end.

The results presented in this paper indicate that the behavior of the flow in the tip gap region of a linear cascade turbine blade depend both on thickness-to-gap and the gap-to-chord ratios. In all cases regardless of the thickness-to-gap, the surface flow visualization revealed a well defined re-attachment line at which the shear direction bifurcates, with some vectors pointed towards the suction side, and others pointed towards the pressure side of the blade. This re-attachment was associated with the flow separation from the pressure-side edge of the blade tip. The re-attachment line never reached to the leading edge of the blade. Rather there was a well delineated portion of the blade at the leading edge at which the shear vectors indicate that the passage flow traversed through the gap without re-attaching.

Given these characteristic features of the surface visualization, as the thickness-to-gap ratio increased, the region where the passage flow traverses through the gap without re-attaching moves further back along the chord of the blade. Commensurate with this was a decrease in the chordwise extent of the re-attachment line. The chordwise extent of the re-attachment line also shortened as the gap-to-chord increased, even for the same thickness-to-gap ratio. This contradicts previous suggestions that "thin" blade behavior lacks a flow re-attachment in the tip-gap region of the blade.

Even though a "thin/thick" regime could not be correlated with the presence or lack of a separation/re-attachment line on the blade end, there was evidence in other features of the tip-gap flow of "thin" and "thick" blade behavior. This appeared in the location from the wall of the maximum loss coefficient associated with the tip-gap vortex, and with the blade-tip loading. Based on these, the boundary between the two regimes is at t/g=3.5, which also agrees with the observations presented in Section 5.

The effect of squealer tips was found to primarily depend on the gap-to-chord ratio. At g/c=0.05, the squealer tip increased the blade tip loading for the full range of the thickness-to-gap ratios, encompassing "thin" and "thick" regimes. The surface flow visualization indicated that a majority of the flow under the blade was turned by the squealer tip, suggesting a large recirculation zone. The chordwise extent of this was comparable to the baseline case. The flow near the leading edge was turned and vectored along the chord direction of the blade, feeding the recirculation zone. This large circulation formed by the squealer is a major drawback of this passive flow control because it could enhance heat transfer that could erode the blade tip. At the higher g/c=0.08, the squealer tip had only a small improvement on the blade tip loading at a smaller t/g that fell within the "thin" regime, but a somewhat larger improvement for the larger t/g that fell in the lower edge of the "thick regime".

Finally, defining the locations of the separation and re-attachment lines is important to our goals of active tip-gap flow control using plasma actuators because such flow features are traditionally highly receptive to unsteady forcing. The ultimate intention is to affect the tip-vortex formation and downstream mixing by exciting an instability of the blade-gap flow by unsteady forcing through a plasma actuator located on the blade tip.

7.0 FIXED MASS AVERAGING RESULTS

In the weeks prior to the final preparation of this report, it was noted that the mass averaged integrals utilized in defining the tip losses were evaluated over an area that was not a fixed mass flux value. It was anticipated that improved comparison and interpretation could be acheived if these integrals were evaluated using a fixed mass flux. Specifically, a capture stream tube in the approach fluid could be considered whose total pressure is uniform over the stream tube area. The size, shape, and total pressure of this stream tube downstream of the cascade section will vary depending on the three dimensional flow structure, and thus will depend on the dependent variables of interest (i.e., gap, thickness, and plasma forcing).

Several of the test cased presented in the previous sections will now be considered using the fixed mass flux integrals. First, the loss coefficients for flat-tip and squealer-tip at g/c=0.05 is shown in Figure 51. The mass flux used for the integration was defined as a region centered around the tip clearance vortex (as noted by the λ_2 contours). For the flat tip case, increasing blade thickness at the tip reduced the total pressure loss coefficient for each thickness-to-gap investigated. Adding a squealer always reduced the total pressure loss. The effects of increase thickness with the squealer tip are less well defined, showing a local minimum at t/g=3.7.

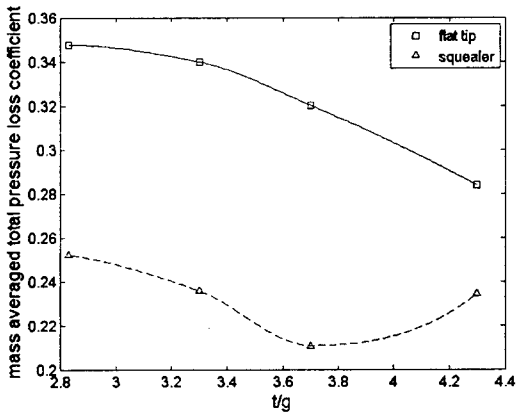

Figure 51 Mass averaged total pressure loss as a function of thickness to gap with and without a squealer tip at a gap-to-chord ratio of 5%

Mass averaged total pressure loss coefficients were determined with fixed mass flux at g/c=0.08. These data are shown in Figure 52. For the flat tip case, increasing blade thickness at the tip reduced the total pressure loss coefficient essentially linearly. At this gap size, however, adding a squealer increased total pressure loss for thickness-to-gap ratios less than 3.5. Near a thickness-to-

gap ratio of 3.5 the total pressure loss for a blade with a squealer saw a sharp decrease with a total pressure coefficient with the squealer lower than that without.

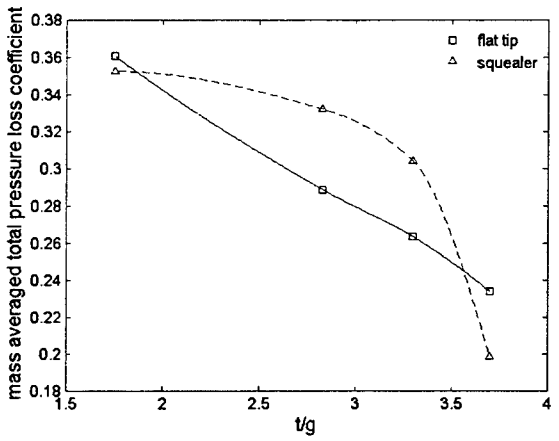

Figure 52 Mass averaged total pressure loss as a function of thickness to gap with and without a squealer tip at a gap-to-chord ratio of 8%

The fixed mass flux integrals were evaluated for the unsteady plasma control cases at g/c=0.04. These data are shown in Figure 53. A total loss reduction of approximately 8% was noted at the higher forcing frequency.

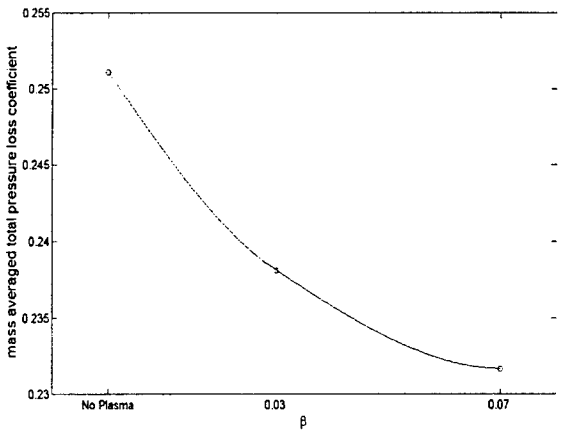

Figure 53 Mass averaged total pressure loss as a function of non-dimensional frequency at a gap-to-chord ratio of 4%

8.0 CONCLUSIONS AND FUTURE WORK

The leakage of fluid over the tip of all rotating machines leads to a reduction in both performance and efficiency. Previously a number of passive flow control designs have been considered, including modifications to the casing as well as the blade tips. For turbine flows, the use of such geometries is complicated by the heat transfer requirements. Specifically, flows which exhibit improved aerodynamic performance often results in a degradation of the thermal properties of the flow field.

The use of active flow control has a number of advantages. The present report describes the first use of active flow control applied directly to the blades themselves. Plasma actuators are ideal for this type of control since they only require a small amount of electrical power in order to produce substantial control benefits. The linear cascade experiments presented have provided significant insight into both passive and active flow control for turbine blades. The following summarized the conclusions that have been made.

1. The tip clearance flow is highly dependent on the thickness to gap ratio. This parameter therefore plays a dominant role in any type of control strategy. The present results have shown that a critical thickness to gap ratio of approximately 3.5 exists for which dramatic changes in the tip behavior are observed. It is assumed that this result is related to the reattachment of separated leakage flow as the blade thickness is increased. This result also provides an explanation as to why the passive control (squealer tip) and active plasma control were found to be ineffective at the smaller gap values. That is, there is a substantially reduced effect of the flow control when the flow does not reattach to the blade end.
2. The "plasma-squealer" was found to be an effective method for controlling the flow through the tip gap in the linear cascade. The large degree of variability in the initial data was determined to be a result of sensitivity to t/g, g/c, as well as the unsteady actuation frequency. Careful mass averaging shown in Section 7 have shown that the losses associated with the tip leakage vortex could be reduced by approximately 8% using unsteady actuation.

It is worth noting that this study was conducted using a single type of actuator geometry that was designed during the early stages of the project. The results presented herein have motivated a number of possible new configurations that may take better advantage of the flow topology that has been observed. For example, unsteady actuation at the point of separation (blade tip pressure side) will likely result in a strong mixing effect in the gap itself. It is expect that this will act as an "aerodynamic blockage" that will aid in turing the core fluid and reducing losses. Other possibili-

ties not considered yet include mounting multiple actuators on the blade surfaces, tip, and endwall in order to provide the maximum control of the secondary flow characteristics.

As a final note, the design of the electrode configuration used in the plasma actuators has received considerable attention. Bench-top type experiments and plasma-gas simulations have shown that new actuators using thick dielectric with low capacitance (e.g., 0.25 inch thick Teflon) provide a net actuator thrust that was 10 to 20 times larger than the actuators used in the experiments presented in this report. Current experiments are underway to determine how these new "high-output" actuators will effect the tip flow physics.

9.0 REFERENCES

Bae, K. Breuer, C. Tan, "Control of Tip Clearance Flows in Axial Compressors," AIAA 2000-2233.

Booth, P. Dodge, H. Hepworth, "Rotor-tip Leakage Part I - BAsic Methodology," ASME 81-GT-71, 1982.

Corke, T., Cavalieri, D., and Matlis, E., Boundary layer instability on a sharp cone at Mach 3.5 with controlled input. AIAA Journal, Vol. 40, No. 5, pp. 1015, 2001.

Corke, E. Matlis, "Phased Plasma Arrays for Unsteady Flow Control," AIAA Paper 2000-2323.

Corke, E. Jumper, M. Post, D. Orlov, T. McLaughlin, "Application of Weakly-ionized Plasmas as Wing Flow-Control Devices, AIAA Paper 2002-0350, submitted to AIAA J.

Corke, T., He, C. and Patel, M., 2004. Plasma flaps and slats: an application of weakly-ionized plasma actuators. AIAA Paper 2004-2127.

Corke, T., Mertz, B. and Patel, M. 2006. Plasma flow control optimized airfoil. AIAA Paper 2006-1208.

Denton, "Loss Mechanisms in Turbomachines," ASME 93-GT-435, 1993.

Dey, "Aerodynamic tip desensitization in axial flow turbines," Ph.D. Thesis, Pen. State University, 2001.

Enloe, L, T. McLaughlin, VanDyken, Kachner, E. Jumper, and T. Corke. 2004. Mechanisms and Response of a single dielectric barrier plasma actuator: Plasma morphology. AIAA J. 42, 3, p. 589. Also AIAA 2003-1021.

Enloe, L, T. McLaughlin, VanDyken, Kachner, E. Jumper, T. Corke. M. Post, O. Haddad. 2004. Mechanisms and Response of a single dielectric barrier plasma actuator: Geometric effects. AIAA J., 42, 3, p 595.

Harvey, K. Ramsden, "A Computational Study of a Novel Turbine Rotor Partial Shroud," *J. Turbomachinery*, Vol. 123, p 534.

Heyes, H. Hodson, G Dailey, "The Effect of Blade Tip Geometry on the Leakage Flow in Axial Turbine Cascades," ASME 91-GT-125, 1991.

Huang, T. Corke, F. Thomas, "Plasma Actuators for Separation Control of Low Pressure Turbine Blades," AIAA Paper 2003-1027.

Huang, J., Corke, T. and Thomas, F. 2006. Unsteady plasma actuators for separation control of low pressure turbine blades. Accepted to appear AIAA J.

Huang, J. 2005. Documentation and control of flow separation on a linear cascade of Pak-B blades using plasma actuators. Ph.D., University of Notre Dame, Notre Dame, Indiana.

N.L. Key, T. Arts, "Comparison of Turbine Tip Leakage Flow for Flat Tip and Squealer Tip Geometries at High-Speed Conditions," ASME GT2004-53979.

McCarter, X. Xiao, and B. Lakshminarayana, "Tip Clearance Effects in a Turbine Rotor: Part 2, Velocity Field and Flow Physics," *J. of Turbomachinery*, Vol. 123, 2001, p305.

Orlov, D., Corke, T., and Patel, M. 2006. Electric circuit model for aerodynamic plasma actuator. AIAA-2006-1206.

Orlov, D., T. Corke, and Haddad, O., 2003. DNS Modeling of plasma actuators. Bulletin of the American Physical Society Fluid Dynamics Division, Annual Meeting.

Orlov, D. and Corke, T. 2005. Numerical simulation of aerodynamic plasma actuator effects. AIAA Paper 2005-1083.

Papa, R.J. Goldstein, F. Gori, "Effects of Tip Geometry and Tip Clearance on the Mass/Heat Transfer From a Large-Scale Gas Turbine Blade," J Turbomachinery, Vol. 125, 2003, p. 90.

Post, M. and T. Corke. 2003. Separation control on high angle of attack airfoil using plasma actuators. AIAA Paper 2003-1024, AIAA J. 42, 11, p. 2177.

Post, M. 2004. Plasma actuators for separation control on stationary and oscillating wings. Ph.D Dissertation, University of Notre Dame.

Post, M. and Corke, T. 2004. Separation control using plasma actuators - stationary and oscillating airfoils. AIAA Paper 2004-0841.

Voikov, V., Corke, T. and Haddad, O. 2004. Numerical simulation of flow control over airfoils using plasma actuators. Bulletin of the American Physical Society Fluid Dynamics Division, Annual Meeting.

Wei, "Significance of Loss Models in Aerothermodynamics Simulation for Axial Turbines," Ph.D. Thesis, Royal Institute of Technology, Sweden.

Xiao, A. McCarter, and B. Lakshminarayana, "Tip Clearance Effects in a Turbine Rotor: Part 1, Pressure Field and Loss," *J. of Turbomachinery*, Vol. 123, 2001, p296.

Yaras, S. Sjolander, "Prediction of tip leakage losses in axial turbines," *J. Turbomachinery*, Vol. 114, 1992.